

# Mappings between reaction-diffusion and kinetically constrained systems: $A + A \leftrightarrow A$ and the FA model have upper critical dimension $d_c = 2$

Robert Jack<sup>1</sup>, Peter Mayer<sup>2</sup> and Peter Sollich<sup>3</sup>

<sup>1</sup> Rudolf Peierls Centre for Theoretical Physics, University of Oxford, 1 Keble Road, Oxford, OX1 3NP, UK

<sup>2</sup> Department of Chemistry, Columbia University, 3000 Broadway, New York, NY 10027, USA

<sup>3</sup> King's College London, Department of Mathematics, London WC2R 2LS, UK

E-mail: rljack@berkeley.edu, pm2214@columbia.edu, peter.sollich@kcl.ac.uk

**Abstract.** We present an exact mapping between two simple spin models: the Fredrickson-Andersen (FA) model and a model of annihilating random walks with spontaneous creation from the vacuum,  $A + A \leftrightarrow 0$ . We discuss the geometric structure of the mapping and its consequences for symmetries of the models. Hence we are able to show that the upper critical dimension of the FA model is two, and that critical exponents are known exactly in all dimensions. These conclusions also generalise to a mapping between  $A + A \leftrightarrow 0$  and the reaction-diffusion system in which the reactions are branching and coagulation,  $A + A \leftrightarrow A$ . We discuss the relation of our analysis to earlier work, and explain why the models considered do not fall into the directed percolation universality class.

The one spin facilitated Fredrickson-Andersen (FA) model [1, 2] has been of interest recently as a simple model that exhibits dynamical heterogeneity [3, 4, 5, 6, 7]. This model has a dynamical critical point at zero temperature that is not characterised by the divergence of any static lengthscale. As such, it represents a possible model of structural glasses, in which dynamical lengthscales seem to be large, but no large static lengthscales have been found [3].

An important advance was made by Whitelam *et al.* [4]. They showed that the master equation of the FA model can be cast in a field-theoretic formalism that resembles a simple reaction-diffusion system with branching and coagulation processes. The dynamical critical point occurs when the density of the diffusing defects vanishes. The properties of the system near the fixed point can then be studied by the powerful methods of the renormalisation group. The analysis of Ref. [4] indicated that fluctuation effects are important below four dimensions and that the model is controlled by the directed percolation (DP) fixed point [8] between two and four dimensions.

In this article we follow Ref. [4] in writing the FA model in a field theoretic language. The overall picture of a zero temperature dynamical fixed point that controls the low temperature scaling remains robust. However, we show that a somewhat hidden symmetry of the FA model means that the fixed point governing the scaling is Gaussian above two dimensions, and identical to that of annihilation-diffusion below two dimensions. Hence the DP fixed point is not relevant to the FA model.

We determine the critical properties of the FA model by means of an exact mapping to a model of diffusing defects that appear in pairs from the vacuum, and annihilate in pairs: we refer to this as the AA (appear and annihilate) model. The mapping holds in all dimensions and at all temperatures. In one dimension the AA model is a (classical) Ising chain with particular single spin dynamics; above one dimension it is more familiar as the reaction-diffusion system  $A + A \leftrightarrow 0$ . The critical properties of the AA model were derived by Cardy and Täuber [9]; by using our mapping we can then apply this derivation to the FA model. The mapping also allows us to identify an (exact) duality symmetry of the FA model, which it inherits from the parity symmetry of the AA model. These symmetries are most simply expressed in terms of the master operators for the stochastic processes, which can also be interpreted as Hamiltonians for quantum spin models [10, 11, 12].

We will show that the mapping from FA to AA models is a specific case of a more general relationship between the reaction-diffusion processes in which the reactions are  $A + A \leftrightarrow 0$  on the one hand and  $A + A \leftrightarrow A$  on the other. (Note the presence of both forward and reverse processes in these reactions.) Our conclusion will be that these two systems are controlled by the same fixed point, and that their critical exponents are therefore identical.

The form of the paper is as follows. We define the FA and AA models in Section 1. Both are models of hard core particles, but have generalisations in which particles can share the same lattice site; we also define these models (which we refer to as ‘bosonic’). The mapping between the FA and AA models is determined by their symmetries: it

has quite a rich geometrical structure, which we discuss in Section 2. In Section 2.2 it is shown that the same mapping also connects the more general reaction-diffusion processes  $A+A \leftrightarrow A$  and  $A+A \leftrightarrow 0$ . An analogous mapping also exists between the corresponding bosonic models (Section 3). In Section 4 we study the critical properties of the various models. We also verify the scaling in three dimensions, where the differences between our predictions and those of Ref. [4] are clearest, by numerical simulation. Finally, we summarise our results in Section 5.

## 1. The models

### 1.1. Model definitions

In this section we introduce several models that we will consider in the remainder of the paper. We define them in terms of microscopic dynamical rules, before outlining the methods by which we represent their master equations and correlation functions.

We begin with the one-spin facilitated Fredrickson-Andersen model [1]. This is referred to simply as ‘the’ FA model in what follows; more general FA models with facilitation by several spins, which exhibit more cooperative behaviour [2], will not be covered here. We define the model in terms of  $N$  binary variables,  $n_i \in \{0, 1\}$ , on a hypercubic lattice in  $d$  dimensions. The Hamiltonian for the system is trivial:

$$E = \sum_i n_i. \quad (1)$$

We refer to a site with  $n = 1$  either as an up-spin or as a ‘defect’; sites with  $n = 0$  are thought of as down spins or ‘empty’. The spins can flip with Metropolis rates if and only if at least one of their neighbours is in the up state. That is, for nearest neighbours  $i$  and  $j$ , we have

$$\begin{aligned} 0_i 1_j &\rightarrow 1_i 1_j, & \text{rate } c, \\ 1_i 1_j &\rightarrow 0_i 1_j, & \text{rate } 1. \end{aligned} \quad (2)$$

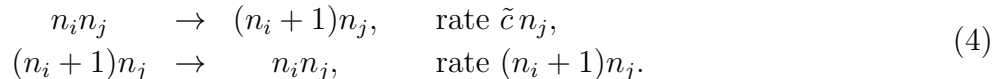
Since we have detailed balance with respect to the Hamiltonian  $E$ , the (dimensionless) rate  $c$  parametrises the temperature according to  $c = e^{-\beta}$ , with  $\beta = 1/T$  as usual. It also sets the equilibrium density

$$\langle n_i \rangle_{\text{FA,eq}} = n_{\text{eq}} \equiv \frac{c}{1+c}. \quad (3)$$

We have introduced the notation  $\langle \cdot \rangle_{\text{FA,eq}}$  for an equilibrium dynamical average.

To avoid confusion, we note that there are other versions of the FA model in the literature. In the original model [1] as described here the rate for flipping a spin  $i$  is proportional to the number of its up-spin neighbours. An alternative definition chooses the rate for flipping spin  $i$  to be independent of the number of neighbours in the up state, as long as there is at least one such neighbour [13]. We do not believe that this choice makes any difference to the critical behaviour of the system, but our exact mappings apply only to the original model as defined above.

We can also define a variant of the FA model in which the occupations  $n_i$  are not restricted to binary values, but may be any non-negative integers. We refer to this as the bosonic FA model, since the natural field theory for describing it has bosonic fields. This model has transition rates



Here and throughout, parameters for the bosonic models are distinguished by tildes from those for the hard core ones. The bosonic model (4) obeys detailed balance with respect to the stationary state  $P(\{n_i\}) = \prod_i e^{-\tilde{c}} \tilde{c}^{n_i} / n_i!$ , so the stationary state density is

$$\langle n_i \rangle_{\widetilde{\text{FA}}, \text{eq}} = \tilde{c}. \quad (5)$$

The bosonic stationary state is again a Gibbs distribution with Hamiltonian  $E$  and temperature defined by  $\tilde{c} = e^{-\beta}$ . However, in contrast to the hard core case it includes an a priori phase space weight factor  $\prod_i 1/n_i!$ , as appropriate for boson statistics.

We will establish a mapping between the FA model and another model of diffusing defects. In this model, defects appear in pairs out of the empty state, and annihilate in pairs into it; they also diffuse freely across the lattice. We refer to this model as the AA model, since the defects appear and annihilate. Both the AA and FA models can be interpreted as reaction-diffusion processes. The AA model has explicit diffusion, combined with reversible annihilation  $A+A \leftrightarrow 0$ . (We follow the standard nomenclature of reaction-diffusion models here, with  $A$  referring to our single species of particles, i.e. defects.) The model is defined for binary variables: for nearest neighbours  $i$  and  $j$ ,



where we choose

$$c' = \frac{\sqrt{1+c}-1}{\sqrt{1+c}+1}, \quad \gamma = \frac{(1+\sqrt{1+c})^2}{2} = \frac{2}{(1-c')^2}. \quad (7)$$

This model also obeys detailed balance with respect to the trivial Hamiltonian,  $E$ , at a temperature parametrised by  $c'$ . Note that, once a trivial overall scale for the rates has been removed, there are in principle two dimensionless rates, and the requirement of detailed balance with respect to  $E$  only fixes one of these, namely the ratio of the rates for appearance and annihilation. For now, we do not let the diffusion rate vary independently and instead tie  $\gamma$  to  $c'$ . The mapping between the FA and AA models will then connect models with the same value of the single parameter  $c$ . The two-parameter generalisation of the AA model with an arbitrary diffusion constant also has a mapping to a generalised FA model, as we discuss in Section 2.2. For notational convenience we study the above ‘standard’ AA and FA models first in what follows.

Finally, there is also a bosonic variant of the AA model with rates

$$\begin{aligned}
 n_i n_j &\rightarrow (n_i - 1)(n_j + 1), & \text{rate } \tilde{\gamma} \tilde{c}' n_i, \\
 n_i n_j &\rightarrow (n_i - 1)(n_j - 1), & \text{rate } \tilde{\gamma} n_i n_j, \\
 n_i n_j &\rightarrow (n_i + 1)(n_j + 1), & \text{rate } \tilde{\gamma} \tilde{c}'^2,
 \end{aligned} \tag{8}$$

where we take  $\tilde{c}' = \tilde{c}/4$  and  $\tilde{\gamma} = 2$ . The stationary state densities in the AA models are

$$\langle n_i \rangle_{\text{AA,eq}} = n'_{\text{eq}} \equiv \frac{c'}{1 + c'}, \quad \langle n_i \rangle_{\widetilde{\text{AA,eq}}} = \tilde{c}'. \tag{9}$$

Note that in the limit of small  $c$ , the relation (7) between  $c'$  and  $c$  becomes  $c' = c/4$ , and thus identical to the one for the bosonic models. More generally, the hard core and bosonic models should become effectively equivalent at low densities where multiple occupancy of sites is very unlikely. We will exploit this correspondence frequently.

### 1.2. Operator forms for the master operators

It is convenient to write stochastic averages for systems such as those defined above in an operator formalism [14]. This is a standard technique, so we largely restrict this section to definitions of the quantities that we will use later.

When considering the bosonic versions of the FA and AA models we use a bosonic algebra with creation and annihilation operators on each site:  $[a_i, a_j] = [a_i^\dagger, a_j^\dagger] = 0$ ;  $[a_i, a_j^\dagger] = \delta_{ij}$ . The state  $\{n_i\}$  is then associated with the vector  $\prod_i (a_i^\dagger)^{n_i} |0\rangle$ , where  $|0\rangle$  is the vacuum state which has all sites empty; the set of all  $2^N$  state probabilities  $P(\{n_i\}, t)$  is mapped to the vector  $|\psi(t)\rangle = \sum_{\{n_i\}} P(\{n_i\}, t) \prod_i (a_i^\dagger)^{n_i} |0\rangle$ . The individual probabilities can be retrieved via  $P(\{n_i\}, t) = \langle 0 | \prod_i (a_i^{n_i} / n_i!) |\psi(t)\rangle$ , and since they must sum to unity one has  $\langle \tilde{e} | \psi(t) \rangle = 1$  where

$$\langle \tilde{e} | = \langle 0 | \prod_i e^{a_i} \tag{10}$$

is a ‘projection state’ that implements the sum over all possible system configurations. The master equation can then be written in operator form as  $\partial_t |\psi(t)\rangle = -\mathcal{L} |\psi(t)\rangle$ , where  $\mathcal{L}$  is known as the Liouvillian or simply the master operator. The off-diagonal elements  $-\langle 0 | \prod_i (a_i^{n'_i} / n'_i!) \mathcal{L} \prod_i (a_i^\dagger)^{n_i} |0\rangle$  of  $-\mathcal{L}$  give the rates for transitions from state  $\{n_i\}$  to  $\{n'_i\}$ , while the diagonal elements follow from the requirement  $\langle \tilde{e} | \mathcal{L} = 0$ . Since the master equation is linear, it can be solved formally as  $|\psi(t)\rangle = e^{-\mathcal{L}t} |\psi(0)\rangle$ . If we specify the initial state as  $\{n_i\}$  we can read off from this the probability of making a transition to state  $\{n'_i\}$  in some time interval  $t$ :

$$P_{\{n'_i\} \leftarrow \{n_i\}}(t) = \langle 0 | \left[ \prod_i \frac{a_i^{n'_i}}{n'_i!} \right] e^{-\mathcal{L}t} \left[ \prod_i (a_i^\dagger)^{n_i} \right] |0\rangle. \tag{11}$$

Expectation values over the stochastic dynamics can also be expressed in a simple form; for example, the average of some function  $f(\{n_i\})$  at time  $t$  becomes

$$\langle f(\{n_i\}) \rangle = \sum_{\{n_i\}} f(\{n_i\}) P(\{n_i\}, t) = \langle \tilde{e} | f(\{\hat{n}_i\}) e^{-\mathcal{L}t} |\psi(0)\rangle, \tag{12}$$

where  $\hat{n}_i = a_i^\dagger a_i$  is particle number operator for site  $i$ . Similar expressions can be written for correlations functions involving two or more times, as illustrated below.

The hard core models with their binary occupation variables  $n_i$  have similar relations but here the states are generated by operators  $s_i^+$  and  $s_i^- \equiv (s_i^+)^\dagger$  in a spin- $\frac{1}{2}$  algebra, with  $(s_i^+)^2 = (s_i^-)^2 = 0$  and  $s_i^+ s_i^- + s_i^- s_i^+ = 1$ . The state vector is now  $|\psi(t)\rangle = \sum_{\{n_i\}} P(\{n_i\}, t) \prod_i (s_i^+)^{n_i} |0\rangle$ , and conversely  $P(\{n_i\}, t) = \langle 0 | \prod_i (s_i^-)^{n_i} |\psi(t)\rangle$ . Conservation of probability requires  $\langle e | \psi(t) \rangle = 1$  with the appropriate projection state now being

$$\langle e | = \langle 0 | \prod_i (1 + s_i^-). \quad (13)$$

Transition probabilities and single-time averages take the forms

$$P_{\{n'_i\} \leftarrow \{n_i\}}(t) = \langle 0 | \left[ \prod_i (s_i^-)^{n'_i} \right] e^{-\mathcal{L}t} \left[ \prod_i (s_i^+)^{n_i} \right] |0\rangle, \quad (14)$$

and

$$\langle f(\{n_i\}) \rangle = \langle e | f(\{\hat{n}_i\}) e^{-\mathcal{L}t} |\psi(0)\rangle, \quad (15)$$

respectively, where now  $\hat{n}_i = s_i^+ s_i^-$ . Occasionally it will be useful to write states and operators in notation analogous to Pauli matrices and spin vectors. Choosing a basis at each site as

$$|\downarrow\rangle_i \equiv |0\rangle_i = \begin{pmatrix} 1 \\ 0 \end{pmatrix}, \quad |\uparrow\rangle_i \equiv |1\rangle_i = \begin{pmatrix} 0 \\ 1 \end{pmatrix}, \quad (16)$$

one has for example

$$s_i^+ = \begin{pmatrix} 0 & 0 \\ 1 & 0 \end{pmatrix}_i, \quad \hat{n}_i = \begin{pmatrix} 0 & 0 \\ 0 & 1 \end{pmatrix}_i. \quad (17)$$

In principle one should write in this expression a direct product  $\bigotimes_{j \neq i} I_j$  with identity operators at all other sites, but for ease of presentation we drop this here and below, along with site subscripts  $i$  where these are clear from the context. Our ordering of the basis states, while the reverse of the usual convention for spins, facilitates comparisons with other work on reaction-diffusion systems [12]. It also emphasises the analogy to the bosonic case, where the only natural ordering of the basis states is in order of increasing occupancy.

It remains to give the forms of the master operator  $\mathcal{L}$  for our models. Their matrix elements are easily derived from the relevant transition rates as explained above. One finds:

$$\mathcal{L}_{\text{FA}} = \sum_{\langle ij \rangle} [(s_i^+ - 1) s_i^- s_j^+ s_j^- s_i^+ (s_i^- - c) + (i \leftrightarrow j)], \quad (18)$$

$$\tilde{\mathcal{L}}_{\text{FA}} = \sum_{\langle ij \rangle} [(a_i^\dagger - 1) a_j^\dagger a_j (a_i - \tilde{c}) + (i \leftrightarrow j)], \quad (19)$$

$$\mathcal{L}_{\text{AA}} = (\gamma/2) \sum_{\langle ij \rangle} [(s_i^+ - 1) s_i^- (s_j^+ + 1) s_j^- s_j^+ (s_j^- + c') s_i^+ (s_i^- - c') + (i \leftrightarrow j)], \quad (20)$$

$$\tilde{\mathcal{L}}_{\text{AA}} = (\tilde{\gamma}/2) \sum_{\langle ij \rangle} \left[ (a_i^\dagger - 1)(a_j^\dagger + 1)(a_j + \tilde{c}') (a_i - \tilde{c}') + (i \leftrightarrow j) \right], \quad (21)$$

where the sums run over all nearest neighbour pairs. The operators  $\mathcal{L}_{\text{FA}}$  and  $\mathcal{L}_{\text{AA}}$  for the hard core models have been written in a suggestive form that emphasises the connection with their bosonic counterparts  $\tilde{\mathcal{L}}_{\text{FA}}$  and  $\tilde{\mathcal{L}}_{\text{AA}}$ .

Before leaving this section, we note that the stationary states of our models have simple closed forms in the quantum formalism, viz.

$$|c\rangle = \prod_i \frac{1 + c s_i^\dagger}{1 + c} |0\rangle \quad \text{and} \quad |\tilde{c}\rangle = \prod_i e^{\tilde{c}(a_i^\dagger - 1)} |0\rangle \quad (22)$$

for the hard core and bosonic case, respectively. The latter is distinguished by a tilde as usual. Correlations in the stationary state then also take a rather simple form. For times  $t_1, \dots, t_k$  that are in increasing order we have

$$\langle n_{i_1}(t_1) n_{i_2}(t_2) \dots n_{i_k}(t_k) \rangle_{\text{FA,eq}} = \langle e | \hat{n}_{i_k} e^{-\mathcal{L}_{\text{FA}}(t_k - t_{k-1})} \hat{n}_{i_{k-1}} \dots \hat{n}_{i_2} e^{-\mathcal{L}_{\text{FA}}(t_2 - t_1)} \hat{n}_{i_1} | c \rangle. \quad (23)$$

The AA model has an identical relation with  $\mathcal{L}_{\text{FA}}$  replaced by  $\mathcal{L}_{\text{AA}}$  and  $c$  replaced by  $c'$ , and for the bosonic models one merely has to substitute for the master operator, projection and stationary state vectors their bosonic equivalents.

## 2. Symmetries and mappings for hard core particles

### 2.1. Detailed balance, parity and duality symmetries

Having set up the operator formalism for dynamics, we now investigate some properties of the Master operators for these models. We first consider the effects of detailed balance, which tells us that the operator  $\mathcal{L}e^{-\beta\hat{E}}$  is Hermitian (or more specifically symmetric, since all matrix elements are real). Here  $\hat{E} = \sum_i \hat{n}_i$  is the (Hermitian) operator for the energy. Multiplying by  $e^{\beta\hat{E}/2}$  from the left and right shows that also

$$H = e^{\beta\hat{E}/2} \mathcal{L} e^{-\beta\hat{E}/2} \quad (24)$$

is Hermitian. This is more useful than  $\mathcal{L}e^{-\beta\hat{E}}$  since it is related to the Liouvillian  $\mathcal{L}$  by a similarity transformation and so has the same eigenvalues. For the FA model we can write explicitly  $e^{-\beta\hat{E}/2} = \prod_i h_i(c)$ , where  $h_i(\cdot)$  is the single site operator

$$h_i(x) = x^{1/2} s_i^+ s_i^- + s_i^- s_i^+ = \begin{pmatrix} 1 & 0 \\ 0 & x^{1/2} \end{pmatrix}. \quad (25)$$

For the AA model we only need to replace  $c$  by  $c'$ . The Hermitian forms of the Liouvillians are then

$$H_{\text{FA}} = \left[ \prod_i h_i^{-1}(c) \right] \mathcal{L}_{\text{FA}} \left[ \prod_i h_i(c) \right], \quad H_{\text{AA}} = \left[ \prod_i h_i^{-1}(c') \right] \mathcal{L}_{\text{AA}} \left[ \prod_i h_i(c') \right]. \quad (26)$$

Their explicit forms make it evident that they are indeed Hermitian: for example

$$H_{\text{FA}} = \sum_{\langle ij \rangle} \left[ (s_i^+ - \sqrt{c}) s_i^- s_j^+ s_j^- s_i^+ (s_i^- - \sqrt{c}) + (i \leftrightarrow j) \right], \quad (27)$$

and  $H_{AA}$  is similarly obtained from  $\mathcal{L}_{AA}$  in (20) by replacing the coefficients  $\pm 1$  and  $\pm c'$  by  $\pm\sqrt{c'}$ .

The above similarity transformation to a Hermitian form of the Liouvillians is convenient since it makes manifest the symmetries and conserved quantities of the systems. The mapping between FA and AA models relies on the fact that the Hermitian operators  $H_{FA}$  and  $H_{AA}$  are related by the *exact* unitary (or, more specifically, orthogonal) transformation

$$H_{FA} = U^{-1}H_{AA}U, \quad (28)$$

where

$$U = \prod_i u_i, \quad u_i = \frac{1}{\sqrt{1+c'}} \left[ 1 - 2i\sqrt{c'}s_i^y \right] = \frac{1}{\sqrt{1+c'}} \begin{pmatrix} 1 & \sqrt{c'} \\ -\sqrt{c'} & 1 \end{pmatrix},$$

with  $s_i^y = (s_i^+ - s_i^-)/2i$  as usual. Equation (28) is the key relation from which most other results for the hard core models are derived; it is easy to verify by direct calculation. The operator  $U$  has a simple geometrical interpretation: it is just a rotation about the  $y$ -axis of the spin sphere, as illustrated in Figure 1 below.

From (28) we have directly a similarity transform between the corresponding master operators for the FA and AA models:

$$\mathcal{L}_{FA} = V^{-1}\mathcal{L}_{AA}V, \quad (29)$$

with

$$V = \prod_i v_i, \quad v_i = \frac{\sqrt{1+c'}}{2} \sqrt{\frac{c}{c'}} h_i(c') u_i h_i^{-1}(c) = \frac{1}{2} \begin{pmatrix} 1 + \sqrt{1+c} & 1 \\ 1 - \sqrt{1+c} & 1 \end{pmatrix}.$$

We have exploited the freedom to introduce an arbitrary prefactor into  $v_i$  to ensure that both its columns add up to unity, i.e.

$$(\langle 0|_i + \langle 1|_i)v_i = \langle 0|_i + \langle 1|_i. \quad (30)$$

For the whole transformation  $V$  this implies that the projection state (13) is invariant under multiplication by either  $V$  or  $V^{-1}$  from the right,  $\langle e|V = \langle e|V^{-1} = \langle e|$ . So (29) automatically maps a probability-preserving Liouvillian onto another one.

Various relations between correlation functions in the two models can now be established. In addition to (30) one uses the analogous property for application of  $v_i$  to the steady state vector on the right:

$$v_i \frac{|0\rangle_i + c|1\rangle_i}{1+c} = \frac{|0\rangle_i + c'|1\rangle_i}{1+c'}, \quad (31)$$

and hence  $V|c\rangle = |c'\rangle$  for the steady state (22). For the simplest connected correlation function one has then, using the definition (23) and the mapping (29),

$$\begin{aligned} & \langle [n_i(t) - n_{\text{eq}}][n_j(0) - n_{\text{eq}}] \rangle_{\text{FA,eq}} \\ &= \langle e|(\hat{n}_i - n_{\text{eq}})e^{-\mathcal{L}_{\text{FA}}t}(\hat{n}_j - n_{\text{eq}})|c\rangle, \\ &= \langle e|V^{-1}[V(\hat{n}_i - n_{\text{eq}})V^{-1}]e^{-\mathcal{L}_{\text{AA}}t}[V(\hat{n}_j - n_{\text{eq}})V^{-1}]V|c\rangle. \end{aligned} \quad (32)$$



Equation (30) implies that the leftmost factor of  $V^{-1}$  can be absorbed into the projection state, while the rightmost factor  $V$  just changes  $c$  to  $c'$  in the steady state vector. Given that the number operators transform as

$$V\hat{n}_iV^{-1} = v_i\hat{n}_iv_i^{-1} = \frac{1}{1+c'} \begin{pmatrix} c' & 1 \\ c' & 1 \end{pmatrix}, \quad (33)$$

one verifies also that

$$(\langle 0|_i + \langle 1|_i)v_i(\hat{n}_i - n_{\text{eq}})v_i^{-1} = \frac{2}{\sqrt{1+c'}}(\langle 0|_i + \langle 1|_i)(\hat{n}_i - n'_{\text{eq}}), \quad (34)$$

and

$$v_j(\hat{n}_j - n_{\text{eq}})v_j^{-1} \frac{|0\rangle_i + c'|1\rangle_i}{1+c'} = \frac{2}{\sqrt{1+c'}}(\hat{n}_j - n'_{\text{eq}}) \frac{|0\rangle_i + c'|1\rangle_i}{1+c'}, \quad (35)$$

so that overall

$$\langle [n_i(t) - n_{\text{eq}}][n_j(0) - n_{\text{eq}}] \rangle_{\text{FA,eq}} = \frac{4}{1+c'} \langle [n_i(t) - n'_{\text{eq}}][n_j(0) - n'_{\text{eq}}] \rangle_{\text{AA,eq}}. \quad (36)$$

It is then a trivial extension to show that for arbitrary connected stationary state correlation functions of a single time difference,

$$\begin{aligned} & \left\langle \left[ \prod_{r=1}^l (n_{i_r}(t) - n_{\text{eq}}) \right] \left[ \prod_{r=1}^m (n_{j_r}(0) - n_{\text{eq}}) \right] \right\rangle_{\text{FA,eq}} \\ &= \left( \frac{4}{1+c} \right)^{(l+m)/2} \left\langle \left[ \prod_{r=1}^l (n_{i_r}(t) - n'_{\text{eq}}) \right] \left[ \prod_{r=1}^m (n_{j_r}(0) - n'_{\text{eq}}) \right] \right\rangle_{\text{AA,eq}}. \end{aligned} \quad (37)$$

However, a direct generalisation to stationary state correlations involving more than one time difference, or out-of-equilibrium quantities depending on more than one time, is not possible. This is because the transformation (33) of the number operator produces a non-diagonal operator which does not directly correspond to a physical observable. Only where the transformed operator is applied either to the projection state on the left, as in (34), or the steady state on the right, as in (35), can such a link be made; otherwise more complicated relations result [15].

The most useful aspect of the mapping (29) is that it will enable us to reveal symmetries of the FA model which are ‘inherited’ from symmetries of the AA model. Specifically, it is clear from the dynamical rules of the AA model that the parity of the total number of particles in the system is conserved. Mathematically, we have that

$$\mathcal{L}_{\text{AA}} = \left[ \prod_i 2s_i^z \right] \mathcal{L}_{\text{AA}} \left[ \prod_i 2s_i^z \right], \quad (38)$$

where  $s_i^z = \hat{n}_i - \frac{1}{2} = \frac{1}{2} \begin{pmatrix} -1 & 0 \\ 0 & 1 \end{pmatrix}$ . Geometrically, the operator  $\prod_i 2s_i^z$  simply produces a rotation of  $\pi$  radians about the  $z$ -axis of the spin sphere.

Since the FA and AA models are related by a similarity transformation, there must be a symmetry of the FA model that is equivalent to the AA parity symmetry. Applying the transformation (29) to equation (38), we arrive at

$$\mathcal{L}_{\text{FA}} = W^{-1} \mathcal{L}_{\text{FA}} W, \quad (39)$$

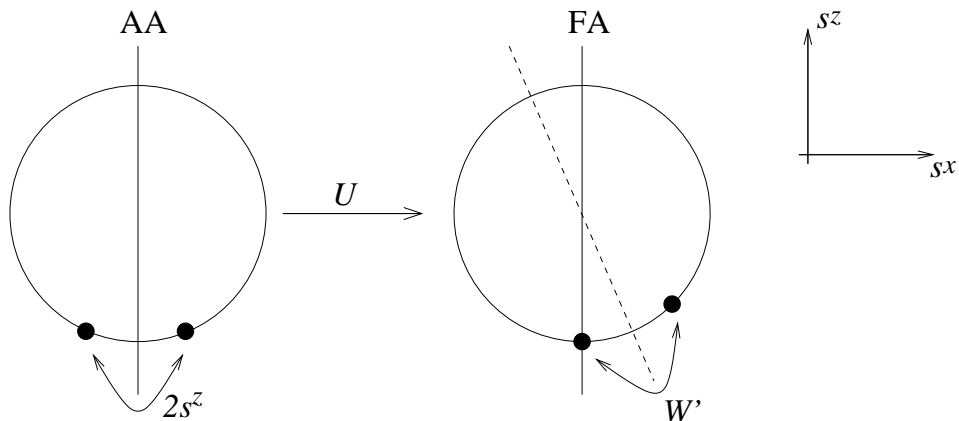


**Figure 1.** The geometrical structure of the mapping  $U$  and the symmetries of the FA and AA models, in terms of the Hermitian operators  $H_{AA}$  and  $H_{FA}$ . Points on the spin sphere represent states  $e^{-i\phi/2} \cos(\theta/2)|\uparrow\rangle + e^{i\phi/2} \sin(\theta/2)|\downarrow\rangle$  where  $\theta$  and  $\phi$  are the usual polar and azimuthal angles. The black dots mark the position on the spin sphere of the zero eigenstates of the operators; these are  $\bigotimes_i (|\downarrow\rangle_i \pm \sqrt{c'}|\uparrow\rangle_i)$  for the AA model, and  $\bigotimes_i (|\downarrow\rangle_i + \sqrt{c'}|\uparrow\rangle_i)$  and  $\bigotimes_i |\downarrow\rangle_i$  for the FA model. Since these states factorise over sites  $i$ , the figure can be read not just schematically as representing the entire  $N$ -spin system, but also literally as showing the spin spheres for a single site. The rotation  $U$  is about the  $y$ -axis of the spin sphere (which points into the paper): it maps  $H_{AA}$  onto  $H_{FA}$ . The rotation  $\prod_i (2s_i^z)$  of  $\pi$  radians about the  $z$ -axis maps  $H_{AA}$  onto itself. Applying the mapping  $U$  gives the duality transformation  $W' = U^{-1}(\prod_i 2s_i^z)U$ , which is a rotation of  $\pi$  radians about the dashed axis and maps  $H_{FA}$  onto itself. In terms of the transformations in the main text,  $W'$  is simply the image  $W$  after mapping  $\mathcal{L}_{FA}$  onto  $H_{FA}$ : we show  $W'$  here since its geometrical structure is simpler.

with

$$W = V^{-1} \left[ \prod_i 2s_i^z \right] V = \prod_i w_i, \quad w_i = v_i^{-1} (2s_i^z) v_i = \frac{1}{\sqrt{1+c}} \begin{pmatrix} -1 & -1 \\ -c & 1 \end{pmatrix}.$$

Note that  $W^{-1} = W$ , as expected for a symmetry deriving from the parity symmetry in the AA model. To understand more closely the effect of  $W$  note first that, in the AA case, the rotation  $\prod_i 2s_i^z$  maps the steady state vector  $|c'\rangle \propto \bigotimes_i (|0\rangle_i + c'|1\rangle_i)$  to the vector  $\bigotimes_i (|0\rangle_i - c'|1\rangle_i)$  where the probabilities of all states  $\{n_i\}$  containing an odd number of particles acquire a negative sign. The sum and difference of these two states gives the physical steady states for initial conditions containing an even and odd number of particles, respectively. In the FA case,  $W$  also maps two steady states onto each other:  $W \bigotimes_i (|0\rangle_i + c|1\rangle_i) \propto |0\rangle = \bigotimes_i |0\rangle_i$ . The symmetry thus links the ‘conventional’ steady state, which is reached for any nonzero initial number of particles, to the vacuum, i.e. the empty state; the latter is trivially a steady state since the kinetic constraints of the FA model forbid any transitions into or out of it. So while the original symmetry in the AA model connects steady states that are basically equivalent, with associated ‘domains of attraction’ of equal size, the inherited symmetry of the FA model relates two very different steady states, with one having a domain of attraction containing *all* configurations except for the empty one.

The above relations between the FA and AA models, and their corresponding symmetries, can also be understood in terms of the associated Hermitian operators. They then have simple geometric interpretations, as shown in Figure 1.

In the following we will continue to refer to ‘the’ steady state of the FA model as the one with nonzero particle density. The symmetry (39) then allows us to relate the dynamics in this steady state to that in near empty configurations. This implies relations between the associated correlation functions. Proceeding as in (32), one has for example

$$\begin{aligned} \langle [n_i(t) - n_{\text{eq}}][n_j(0) - n_{\text{eq}}] \rangle_{\text{FA,eq}} &= \langle e | W^{-1} [W(\hat{n}_i - n_{\text{eq}})W^{-1}] e^{-\mathcal{L}_{\text{FA}}t} [W(\hat{n}_j - n_{\text{eq}})W^{-1}] W | c \rangle, \\ &= \langle 0 | [W(\hat{n}_i - n_{\text{eq}})W^{-1}] e^{-\mathcal{L}_{\text{FA}}t} [W(\hat{n}_j - n_{\text{eq}})W^{-1}] | 0 \rangle. \end{aligned} \quad (40)$$

Here we have used that application of  $W$  to the steady state vector  $|c\rangle$  on the right gives a multiple of the vacuum state. The same is easily checked for the operation of  $W^{-1}$  on the projection state  $\langle e|$  on the left; the associated proportionality factors cancel because of overall normalisation. The transformation of the number operators is

$$W(\hat{n}_i - n_{\text{eq}})W^{-1} = w_i(\hat{n}_i - n_{\text{eq}})w_i^{-1} = \frac{1}{1+c} \begin{pmatrix} 0 & -1 \\ -c & 1-c \end{pmatrix} = \frac{-cs_i^+ - s_i^- + (1-c)\hat{n}_i}{1+c},$$

so that

$$\langle [n_i(t) - n_{\text{eq}}][n_j(0) - n_{\text{eq}}] \rangle_{\text{FA,eq}} = \langle 0 | \left( -\frac{s_i^-}{1+c} \right) e^{-\mathcal{L}_{\text{FA}}t} \left( -\frac{cs_j^+}{1+c} \right) | 0 \rangle. \quad (41)$$

Up to the overall numerical factor  $c/(1+c)^2$ , the right hand side is of same form as (14): it is the probability of a transition between particular initial and final states, containing a single particle on sites  $j$  and  $i$  respectively. This relation generalises straightforwardly to correlation functions involving more than two spatial points: we have that

$$\begin{aligned} \left\langle \left[ \prod_{r=1}^l (n_{i_r}(t) - n_{\text{eq}}) \right] \left[ \prod_{r=1}^m (n_{j_r}(0) - n_{\text{eq}}) \right] \right\rangle_{\text{FA,eq}} &= \frac{(-1)^{l+m} c^m}{(1+c)^{l+m}} \langle 0 | \left[ \prod_{r=1}^l s_{i_r}^- \right] e^{-\mathcal{L}_{\text{FA}}t} \left[ \prod_{r=1}^m s_{j_r}^+ \right] | 0 \rangle, \end{aligned} \quad (42)$$

where the right hand side is again of the form (14) and gives the transition probability between an initial state with  $m$  particles and a final state with  $l$  particles. While this relation may not be familiar, it is closely related to the duality symmetry of the DP fixed point [8]. The latter is more usually expressed in terms of the dynamical action: see Section 4.

In summary, we see that the transformation  $V$  maps the parity symmetry of the AA model onto an (exact) duality symmetry of the FA model. The mapping thus exposes a hidden symmetry which would not easily be recognised by looking at the FA model alone.

## 2.2. Models with additional diffusive processes

The discussion so far has considered the FA and AA models, both defined in terms of a single parameter  $c$ . We now generalise our arguments to models with extra diffusive processes. This will show that our mapping applies more broadly between reaction-diffusion models with, respectively, reversible coagulation (i.e. coagulation and branching) and reversible annihilation (i.e. annihilation and appearance) processes. The generalised models will also allow us to elucidate the connection between our mapping and related earlier studies.

Consider supplementing the FA model by an additional process



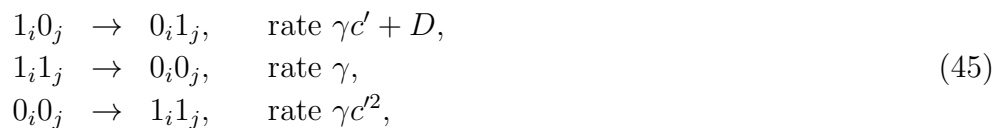
In particle language this is diffusion of a particle  $A$  to a vacant site, while the original processes (2) are  $A \rightarrow A+A$  (branching) and  $A+A \rightarrow A$  (coagulation). This generalised FA model can therefore also be viewed as the reaction-diffusion model  $A + A \leftrightarrow A$ .

The new diffusion term in the master operator can be written as

$$\begin{aligned} \mathcal{L}_{\text{diff}} &= D \sum_{\langle ij \rangle} (s_i^+ - s_j^+) s_i^- s_j^- s_j^+ s_i^+ (s_i^- - s_j^-), \\ &= -2D \sum_{\langle ij \rangle} [s_i^x s_j^x + s_i^y s_j^y + s_i^z s_j^z - 1/4], \end{aligned} \quad (44)$$

where  $s_i^x = (s_i^+ + s_i^-)/2$  and, as before,  $s_i^y = (s_i^+ - s_i^-)/2i$  and  $s_i^z = \hat{n}_i - 1/2 = (s_i^+ s_i^- - s_i^- s_i^+)/2$ . We recognise in (44) the Heisenberg model: see Ref. [10] for a summary of the links between the properties of stochastic systems and their corresponding quantum spin Hamiltonians.

For our purposes it is important to recognise that  $\mathcal{L}_{\text{diff}}$  has nonzero matrix elements only between states containing equal numbers of particles; it is therefore invariant under transformation with  $\prod_i h_i(x)$  – so that the associated Hermitian operator is identical to  $\mathcal{L}_{\text{diff}}$  – and under the parity transformation  $\prod_i 2s_i^z$ . Due to its Heisenberg form,  $\mathcal{L}_{\text{diff}}$  is also left invariant by any global spin rotation, and in particular by  $U$ . Combining these properties, invariance under  $V$  and  $W$  then also follow. Hence the structure of the preceding subsection is all preserved for the generalised models: the generalised FA model with diffusion rate  $D$ , branching rate  $c$  and coagulation rate 1 maps via  $V$  onto a generalised AA model with rates



where  $\gamma$  and  $c'$  depend only on  $c$ , as defined in (7). We note that all generalised FA models have conjugate AA models, but that AA models in which the rate for the diffusive process is less than  $\gamma c'$  cannot be mapped to FA models with positive rates.

At this point, we make contact with two earlier studies. Krebs *et al.* [11] studied the above generalised models at zero temperature but with nonzero  $D$ . Consistent with this, their mapping between the models is the limit of our mapping  $V$  for  $c, c' \rightarrow 0$ .

Henkel *et al.* [12] implicitly had the full mapping  $V$ , but considered it only in the context of one-dimensional systems that are solvable by free fermions. The AA model then reduces to the Glauber-Ising chain (their model IV) and the relevant generalised FA model has  $D = 1$  (their model II). Henkel *et al.* did not comment that the mapping applies to all dimensions and to arbitrary values of the diffusion constant.

We illustrate the relation between our work and Refs. [11] and [12] in Figure 2. We parametrise the FA ( $A + A \leftrightarrow A$ ) models by the ratio of branching and coagulation rates  $c$  and the ratio of diffusion and coagulation rates  $D$ . In the AA case, appropriate dimensionless parameters are the ratio of appearance and annihilation rates  $c'^2$  and the ratio of diffusion and annihilation rates  $D' = c' + D/\gamma$ . All generalised FA models map onto generalised AA models with  $c' < 1$  and  $D' \geq c'$ . The standard FA model is  $D = 0$ , giving  $D' = c'$ , while the pure coagulation/annihilation models of Ref. [11] correspond to  $c = c' = 0$ . The free fermion condition of Ref. [12], finally, is the line  $D = 1$  which maps onto the Glauber-Ising line  $D' = (1 + c'^2)/2$ . (The Glauber-Ising chain has diffusion rate  $1/2$  and annihilation rate  $(1 + c'^2)^{-1}$ , giving the stated ratio.)

To see the explicit link between our mapping and that of Ref. [12], one notes that their free-fermion quantum Hamiltonian is directly in the form of the Liouvillian  $\mathcal{L}_{AA}$  for the AA model if its parameters are chosen as  $D_1 = D_2 = 1$ ,  $h_1 = h_2 = (1 - c'^2)/(1 + c'^2)$ ,  $\eta_1 = 2/(1 + c'^2)$  and  $\eta_2 = \eta_1 c'^2$ . Henkel *et al.* [12] then show that the FA Liouvillian can be obtained by the similarity transformation  $\mathcal{L}_{FA} = B\mathcal{L}_{AA}B^{-1}$ , with  $B = \prod_i b_i$  and

$$b_i = \begin{pmatrix} \sqrt{a} & 0 \\ 0 & 1/\sqrt{a} \end{pmatrix} \begin{pmatrix} \cosh \phi & \sinh \phi \\ \sinh \phi & \cosh \phi \end{pmatrix} \begin{pmatrix} b & 0 \\ 0 & 1/b \end{pmatrix}. \quad (46)$$

Following through their analysis gives  $a = e^{\pi/2} c^{-1/2}$ ,  $b = e^{-\pi/4} c^{1/4}$  and  $\phi = i\theta$ , where  $\tan 2\theta = \sqrt{c}$ . The latter condition can also be written as  $\tan \theta = \sqrt{c'}$ , so that  $\theta$  is in fact the rotation angle associated with our mapping  $U$ . Inserting these values one has  $b_i \propto v_i^{-1}$  (with proportionality factor  $[(1+c)/4]^{1/4}$ ) as expected by comparison with our Equation (29). We note that Henkel *et al.* associate particles with *down* spins rather than up spins as here. However, because they also use the opposite (i.e., conventional) ordering of the two local basis vectors  $|\uparrow\rangle$  and  $|\downarrow\rangle$ , the matrix representations of all operators are the same.

To summarise, we showed in this section that the FA and AA models have quite a rich geometric structure underlying their symmetries and the relations between them. These relations further extend to a general mapping between reaction-diffusion models with coagulation and branching ( $A + A \leftrightarrow A$ ) and annihilation and appearance ( $A + A \leftrightarrow 0$ ). We expect the critical behaviour (at small particle densities, i.e. low temperature) of these models to be determined by their symmetry properties. However, the hard core constraint that allows only one particle per site makes an explicit renormalisation group analysis of such critical properties awkward. We therefore show next that the bosonic models, where this constraint is removed, have analogous symmetries and mappings between coagulation and annihilation models.

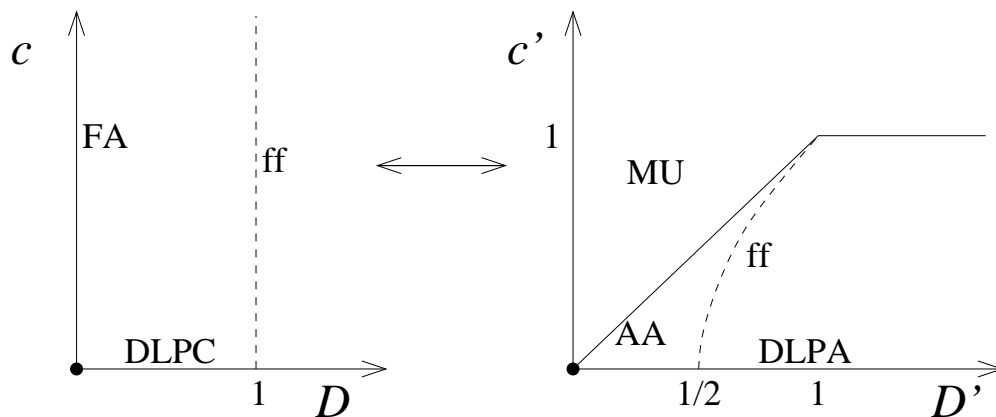


**Figure 2.** Sketch of the mapping between the two-parameter families of generalised FA ( $A + A \leftrightarrow A$ ) and AA ( $A + A \leftrightarrow 0$ ) models. Generalised FA models (with non-negative  $c$ ) map onto generalised AA models with  $0 \leq c' < 1$  and  $c' \leq D'$ . The standard FA models with  $D = 0$  map to models on the standard AA line  $c' = D'$ . The lines  $c = 0$  and  $c' = 0$  correspond to diffusion-limited pair annihilation (DLPA) and diffusion-limited pair coagulation (DLPC) respectively [11]. In one dimension the models are solvable by free fermions on the lines marked ‘ff’. These lines are given by  $D = 1$  and  $D' = (1 + c'^2)/2$ , and the mapping transforms them into each other [12]. In the region marked MU the mapping is unphysical: such generalised AA models do not have FA counterparts with positive rates, though it seems unlikely that this would have physical consequences for the behaviour of the corresponding AA model.

### 3. Bosonic models

The bosonic models introduced in Section 1 have similar properties to those discussed for hard core (spin) models in the previous section. The Liouvillians again have Hermitian analogues defined by  $H = e^{\beta \hat{E}/2} \mathcal{L} e^{-\beta \hat{E}/2}$ . The energy operator is now  $\hat{E} = \sum_i a_i^\dagger a_i$ , so if we define the bosonic version of  $h_i(x)$  as

$$\tilde{h}_i(x) = x^{a_i^\dagger a_i/2}, \quad (47)$$

then

$$\tilde{H}_{\text{FA}} = \left[ \prod_i \tilde{h}_i^{-1}(\tilde{c}) \right] \tilde{\mathcal{L}}_{\text{FA}} \left[ \prod_i \tilde{h}_i(\tilde{c}) \right], \quad \tilde{H}_{\text{AA}} = \left[ \prod_i \tilde{h}_i^{-1}(\tilde{c}') \right] \tilde{\mathcal{L}}_{\text{FA}} \left[ \prod_i \tilde{h}_i(\tilde{c}') \right]. \quad (48)$$

$\tilde{H}_{\text{FA}}$  has the same form as (19) except that the numerical constants 1 and  $\tilde{c}$  are replaced by  $\sqrt{\tilde{c}}$ , i.e.

$$\tilde{H}_{\text{FA}} = \sum_{\langle ij \rangle} [(a_i^\dagger - \sqrt{\tilde{c}}) a_j^\dagger a_j (a_i - \sqrt{\tilde{c}}) + (i \leftrightarrow j)], \quad (49)$$

and  $\tilde{H}_{\text{AA}}$  is obtained similarly from (21). This is analogous to the hard core case, but easier to see for the bosonic models since the transformation by  $h_i(x)$  simply rescales particle creation and annihilation operators, according to the first of the relations

$$e^{\lambda a^\dagger a} F(a, a^\dagger) e^{-\lambda a^\dagger a} = F(e^{-\lambda} a, e^\lambda a^\dagger), \quad (50)$$

$$e^{\lambda a + \mu a^\dagger} F(a, a^\dagger) e^{-\lambda a - \mu a^\dagger} = F(a - \mu, a^\dagger + \lambda). \quad (51)$$

One expects that at low particle densities  $n_{\text{eq}} = c/(1+c) \approx c$  the constraint of at most single occupancy in the hard core FA model will be irrelevant, so that it becomes equivalent to the corresponding bosonic model with  $\tilde{c} = c$ ; the same argument applies to the hard core and bosonic AA models. This physical reasoning [4] can be further supported by a large- $S$  expansion of the hard core models (Appendix A).

We now discuss the mappings between the bosonic models and their symmetries. The main conclusion is that the structure of the hard core models is preserved in their bosonic counterparts. The basic mapping between the two bosonic Hermitian operators is

$$\tilde{H}_{\text{FA}} = \tilde{U}^{-1} \tilde{H}_{\text{AA}} \tilde{U}, \quad (52)$$

with the unitary operator

$$\tilde{U} = \prod_i \tilde{u}_i, \quad \tilde{u}_i = e^{(a_i - a_i^\dagger)\sqrt{\tilde{c}}/2}. \quad (53)$$

This is easy to verify, bearing in mind that  $\tilde{c}' = \tilde{c}/4$  and  $\tilde{\gamma} = 2$ : from (51), the transformation by  $\tilde{U}$  shifts all  $a_i$  and  $a_i^\dagger$  in  $\tilde{H}_{\text{AA}}$  by  $-\sqrt{\tilde{c}}/2 = -\sqrt{\tilde{c}'}$ . If one uses a basis of bosonic coherent states then the mapping is a translation in the complex plane that parametrises these states. This is the analogue of the rotation of the spin sphere generated by  $u_i$ , consistent with the intuition (Appendix A) that the bosonic models effectively ‘flatten’ the spin sphere onto the complex plane of coherent states.

Combining  $\tilde{u}_i$  and  $\tilde{h}_i$  we have a relation between the Liouvillians,

$$\tilde{\mathcal{L}}_{\text{FA}} = \tilde{V}^{-1} \tilde{\mathcal{L}}_{\text{AA}} \tilde{V}, \quad \tilde{V} = \prod_i \tilde{v}_i, \quad \tilde{v}_i = \tilde{h}_i(\tilde{c}') \tilde{u}_i \tilde{h}_i^{-1}(\tilde{c}) = 2^{-a_i^\dagger a_i} e^{(a_i - \tilde{c} a_i^\dagger)/2}, \quad (54)$$

where the explicit form of  $v_i$  follows using (50) and (51). These relations also show that the transformation by  $V$  is simply a combined shift and rescaling of the bosonic operators

$$\tilde{V}^{-1} a_i \tilde{V} = \frac{1}{2} \left( a_i - \frac{\tilde{c}}{2} \right), \quad \tilde{V}^{-1} a_i^\dagger \tilde{V} = 2 \left( a_i^\dagger - \frac{1}{2} \right). \quad (55)$$

The mapping between the two Liouvillians again relates the parity symmetry of the bosonic AA model,

$$\tilde{\mathcal{L}}_{\text{AA}} = (-1)^{\sum_i a_i^\dagger a_i} \tilde{\mathcal{L}}_{\text{AA}} (-1)^{\sum_i a_i^\dagger a_i}, \quad (56)$$

to the duality symmetry of the bosonic FA model

$$\tilde{\mathcal{L}}_{\text{FA}} = \tilde{W}^{-1} \tilde{\mathcal{L}}_{\text{FA}} \tilde{W}, \quad \tilde{W} = \tilde{V}^{-1} (-1)^{\sum_i a_i^\dagger a_i} \tilde{V}. \quad (57)$$

One finds explicitly

$$\tilde{W} = \tilde{W}^{-1} = \prod_i (-1)^{a_i^\dagger a_i} e^{a_i - \tilde{c} a_i^\dagger}, \quad (58)$$

and the duality symmetry transforms the bosonic operators as

$$\tilde{W}^{-1} a_i \tilde{W} = \tilde{c} - a_i, \quad \tilde{W}^{-1} a_i^\dagger \tilde{W} = 1 - a_i^\dagger. \quad (59)$$

The mappings  $\tilde{V}$  and  $\tilde{W}$  allow us to establish the analogues of (37) and (42). The first of these relates steady state correlations in the bosonic FA and AA models via

$$\begin{aligned} & \left\langle \left[ \prod_{r=1}^l (n_{i_r}(t) - \tilde{c}) \right] \left[ \prod_{r=1}^m (n_{j_r}(0) - \tilde{c}) \right] \right\rangle_{\tilde{\text{FA}}, \text{eq}} \\ &= 2^{l+m} \left\langle \left[ \prod_{r=1}^l (n_{i_r}(t) - \tilde{c}') \right] \left[ \prod_{r=1}^m (n_{j_r}(0) - \tilde{c}') \right] \right\rangle_{\tilde{\text{AA}}, \text{eq}}. \end{aligned} \quad (60)$$

Here the  $i_r$  must label sites that are all distinct from each other, as do the  $j_r$ , though the two sets may contain sites in common with each other. The prefactor on the right agrees with the low density limit of the one in (37), supporting our intuition about the equivalence of hard core and bosonic models in this regime.

The duality symmetry of the bosonic FA model results in

$$\begin{aligned} & \left\langle \left[ \prod_{r=1}^l (n_{i_r}(t) - \tilde{c}) \right] \left[ \prod_{r=1}^m (n_{j_r}(0) - \tilde{c}) \right] \right\rangle_{\tilde{\text{FA}}, \text{eq}} \\ &= (-1)^{l+m} \tilde{c}^m \langle 0 | \left[ \prod_{r=1}^l a_{i_r} \right] e^{-\tilde{\mathcal{L}}_{\text{FA}} t} \left[ \prod_{r=1}^m a_{j_r}^\dagger \right] | 0 \rangle. \end{aligned} \quad (61)$$

This again relates steady state correlations to transition probabilities between specific initial and final states; the prefactor approaches the one in (42) for  $c = \tilde{c} \rightarrow 0$ .

Following our discussion in Section 2.2, one expects that the structure of the bosonic mapping will be preserved if an extra diffusive process is added to both models. This is easily verified. It is also immediate to show that the mapping is unchanged if we add on-site branching and coagulation processes, as long as we retain detailed balance for the whole model. These processes then map to on-site appearance and annihilation in the generalised AA model. (Recall that our standard bosonic FA and AA models have processes that always act on pairs of sites.)

The similarities between Eqs (47-61) and (25-39) show clearly that the bosonic models have the same structure as those with hard core exclusion. In the next section we consider the critical properties of these bosonic models; from our arguments the critical properties of the hard core models should be identical, and we check this by comparing our predictions to numerical simulation.

#### 4. Critical properties

We have shown that the FA and AA models are linked by an exact mapping. Now, both models have scaling behaviour at small defect densities that is characterised by the fixed point of a renormalisation group (RG) flow. In Section 4.1 we use the mapping of the previous section together with known results to show that the FA model has upper critical dimension  $d_c = 2$ ; this conclusion also applies to the generalised FA model, i.e. the reaction-diffusion model  $A + A \leftrightarrow A$ . The critical scaling is then characterised by the well-known mean-field (Gaussian) exponents in  $d > 2$ ; we also derive exact exponents



below  $d_c$  that coincide with known results in one dimension. Our results differ from earlier studies in two and three dimensions: in Section 4.2 we therefore use simulations to confirm the predicted mean-field scaling in  $d = 3$ . In Section 4.3 we derive some analytical results for the scaling limit of correlation functions in  $d > 2$ . Finally we discuss in Section 4.4 the scaling of the persistence function since data for this were used in Ref. [4] to support the argument that non-mean-field fluctuation corrections are significant in three dimensions.

#### 4.1. Renormalisation group analysis

The critical properties of the bosonic AA model were established by Cardy and Täuber [9]: in their notation the model corresponds to  $k = 2$ ,  $\tau > 0$ ,  $\sigma_m = 0$ . We write the generating functional for dynamical correlations in the stationary state as a path integral on the lattice

$$Z_{AA} = \int \mathcal{D}[\{\varphi_{it}\}, \{\varphi_{it}^\dagger\}] e^{-\int dt \{[\sum_i \varphi_{it}^\dagger \partial_t \varphi_{it}] + L_{AA}[\{\varphi_{it}\}, \{\varphi_{it}^\dagger\}]\}} \quad (62)$$

where  $\varphi_{it}$  and  $\varphi_{it}^\dagger$  are time-dependent conjugate fields at each site  $i$ . The ‘Lagrangian’  $L_{AA}[\{\varphi_{it}\}, \{\varphi_{it}^\dagger\}]$  is obtained from  $\mathcal{L}_{AA}$  by replacing  $a_i \rightarrow \varphi_{it}$  and  $a_i^\dagger \rightarrow \varphi_{it}^\dagger$ . and depends on all the fields at a single time.

Taking the continuum limit, the lattice fields  $\{\varphi_{it}\}$  are promoted to a field  $\phi_{xt}$  depending on spatial position  $x$  and time  $t$ . The generating functional becomes

$$Z_{AA} = \int \mathcal{D}[\phi_{xt}, \phi_{xt}^\dagger] e^{-S_{AA}[\phi_{xt}, \phi_{xt}^\dagger]} \quad (63)$$

where the functional  $S_{AA}$  is known as the dynamical action. Including gradient terms up to second order gives

$$S_{AA}[\phi, \phi^\dagger] = \int d^d x dt \phi_{xt}^\dagger \partial_t \phi_{xt} + \lambda_0 (\phi_{xt}^\dagger - 1)(\phi_{xt} - \rho')(1 + l_0^2 \nabla^2 / 2)(\phi_{xt}^\dagger + 1)(\phi_{xt} + \rho') \quad (64)$$

where we have neglected boundary terms;  $\rho'$  is the steady state density (proportional to  $\check{c}$ ),  $l_0$  is the microscopic lengthscale (lattice spacing) and  $\lambda_0$  is a bare coupling constant that sets the microscopic timescale. The dimensions of  $\lambda_0$  are  $[\text{time}]^{-1}[\text{length}]^d$ ; the field  $\phi^\dagger$  is chosen to be dimensionless and  $\phi$  has dimension of  $[\text{length}]^{-d}$ .

While the above factorised form for the action was useful for the exact mappings of the previous sections, the RG calculation requires us to separate the terms in the action that correspond to different physical processes. We write

$$S_{AA}[\phi, \phi^\dagger] = \int d^d x dt \left\{ \phi_{xt}^\dagger (\partial_t - \lambda_0 \rho' l_0^2 \nabla^2) \phi_{xt} + \lambda_0 [(\phi_{xt}^\dagger)^2 - 1](\phi_{xt}^2 - \rho'^2) + L_{AA,1} \right\} \quad (65)$$

where

$$L_{AA,1} = (\lambda_0 l_0^2 / 2) [\phi_{xt}^\dagger \phi_{xt} \nabla^2 \phi_{xt}^\dagger \phi_{xt} + (\nabla \phi_{xt})^2 + (\rho' \nabla \phi_{xt}^\dagger)^2] \quad (66)$$

(we continue to ignore boundary terms when integrating by parts over spatial degrees of freedom). Physically, we recognise the first term in (65) as a diffusive propagator

for the excitations and the second term as local appearance and annihilation processes. The terms contained in  $L_{AA,1}$  will be irrelevant in the RG sense since their only effect is to enforce the fact that appearance and annihilation of excitations take place on pairs of adjacent sites and not on single sites. (In terms of the RG calculation these terms modify the spatial structure of terms in the action that are already present, but they are not responsible for new terms, or for any singular behaviour.) We therefore neglect  $L_{AA,1}$  and arrive at the action considered in Ref. [9] for the case ( $k = 2$ ,  $\tau > 0$ ,  $\sigma_m = 0$ ) described above.

We now follow Ref. [9] in renormalising this dynamical action. The parity symmetry of the bosonic AA model is

$$S_{AA}[\phi_{xt}, \phi_{xt}^\dagger] = S_{AA}[-\phi_{xt}, -\phi_{xt}^\dagger], \quad (67)$$

and must not be obscured by making any shift of the fields [9]. The symmetry is clearly preserved under the RG flow so only terms in the action with this symmetry need be considered. Power counting then shows that the upper critical dimension will be two. Above  $d = 2$ , therefore, the critical exponents have their mean-field values

$$(z, \nu, \beta)_{d>2} = (2, 1/2, 1). \quad (68)$$

Here we have defined  $\beta$  by the scaling of the steady-state density  $\lim_{t \rightarrow \infty} \langle n_i(t) \rangle \sim \rho'^\beta$ , and  $\nu$  by the correlation length scaling  $\xi \sim \rho'^{-\nu}$ . (The notation  $a \sim b$  means that  $a$  is proportional to  $b$  in the scaling limit, i.e. close to the critical point at  $\rho' = 0$ .) Note that in Ref. [9] these exponents were defined in terms of the control parameter  $\tau \sim \rho'^2$  and thus differ by factors of two from ours. Our convention is more appropriate for comparison with the FA model, where the steady-state particle density is the natural control parameter. We also note that the free propagator and hence the bare diffusion constant  $D_0$  (the constant multiplying the term  $\phi^\dagger \nabla^2 \phi$  in the action) depend explicitly on  $\rho'$ . In the usual RG analysis  $D_0$  is set to unity, so we define the exponent  $z$  via the scaling of typical relaxation timescales  $\tau$  measured in units of  $D_0^{-1}$ ,

$$D_0 \tau \sim \xi^z \sim \rho'^{-z\nu}. \quad (69)$$

The scaling of the times  $\tau$  in absolute units is then governed by an exponent different from  $z$ :  $D_0 \propto \rho'$  gives

$$\tau \sim \xi^z / D_0 \sim \rho'^{-1-z\nu}. \quad (70)$$

We next show that below  $d = 2$  the exponents are exactly

$$(z, \nu, \beta)_{d<2} = (2, 1/d, 1). \quad (71)$$

This is consistent with the exact scaling in one dimension and also with the naive scaling estimate  $\tau \sim c^{-1-2/d}$  for the FA model [2]. In Ref. [9],  $\nu$  and  $\beta$  were given only to first order in a loop expansion: in our notation the results were

$$z = 2, \quad \beta = d\nu, \quad \nu = 2/y_\tau = 1/d + \mathcal{O}(2-d)^2, \quad (72)$$

for  $d < 2$ . Here  $y_\tau = 2d + \mathcal{O}(2-d)^2$  is the scaling dimension of the coupling  $\tau \sim \rho'^2$ . (The relation  $\beta = d\nu$  comes from the scaling relation  $\beta = z\nu/\alpha$  where  $\alpha$  is the exponent

for the decay of the density after a quench to criticality, which equals  $d/2$  [9].) However, we can determine  $y_\tau$  exactly since detailed balance fixes the steady-state density to the value  $\tilde{c}' \propto \rho'$ , so that  $\beta = 1$ . Thus we have the exact result  $\nu = 1/d$ , or

$$y_\tau = 2d, \quad (73)$$

and the exponents (71) are exact. Equation (73) can be confirmed by summing the geometric series of loop corrections that contribute to the scaling dimension  $y_\tau$ .

Proceeding to the bosonic FA model, the (unshifted) dynamical action is [4]

$$S_{\text{FA}} = \int d^d x dt \phi_{xt}^\dagger \partial_t \phi_{xt} + \mu_0 (\phi_{xt}^\dagger - 1) (\phi_{xt} - \rho) (1 + l_0^2 \nabla^2 / 2) \phi_{xt}^\dagger \phi_{xt}, \quad (74)$$

where  $\rho \propto \tilde{c}$  is the steady state density and  $\mu_0$  is the bare coupling (with dimension  $[\text{time}]^{-1} [\text{length}]^d$ );  $l_0$  is the microscopic lengthscale as before. The property of detailed balance manifests itself as an invariance of the action,

$$S_{\text{FA}}[\phi_{xt}, \phi_{xt}^\dagger] = S_{\text{FA}}[\rho \phi_{x,-t}^\dagger, \rho^{-1} \phi_{x,-t}]. \quad (75)$$

This of course has an analogue in our earlier operator notation, where we recognised detailed balance as the fact that  $\tilde{\mathcal{L}}_{\text{FA}} \exp(-\beta \hat{E})$  is Hermitian. Since  $\exp(-\beta \hat{E}) = \tilde{c}^{\sum_i a_i^\dagger a_i}$ , this implies  $\exp(-\tilde{\mathcal{L}}_{\text{FA}} t) = \tilde{c}^{-\sum_i a_i^\dagger a_i} \exp(-\tilde{\mathcal{L}}_{\text{FA}}^\dagger t) \tilde{c}^{\sum_i a_i^\dagger a_i}$  which is the promised analogue of (75) [recall (50) and note that  $f^\dagger(a, a^\dagger) = f(a^\dagger, a)$ ].

The duality symmetry as it is normally stated for systems with a DP fixed point (but not necessarily with detailed balance) is [8]

$$S_{\text{FA}}[\phi_{xt}, \phi_{xt}^\dagger] = S_{\text{FA}}[\rho(1 - \phi_{x,-t}^\dagger), 1 - \rho^{-1} \phi_{x,-t}]. \quad (76)$$

Like detailed balance this involves time reversal; in terms of the Liouvillian it relates  $\tilde{\mathcal{L}}_{\text{FA}}$  to its conjugate  $\tilde{\mathcal{L}}_{\text{FA}}^\dagger$ . To arrive at the duality mapping for the FA model, we combine the preceding two symmetries of the action to obtain

$$S_{\text{FA}}[\phi_{xt}, \phi_{xt}^\dagger] = S_{\text{FA}}[\rho - \phi_{x,t}, 1 - \phi_{x,t}^\dagger]. \quad (77)$$

In terms of operators, this symmetry now relates  $\tilde{\mathcal{L}}_{\text{FA}}$  directly to itself, without any conjugation. A comparison with (59) reveals that it corresponds directly to our earlier transformation  $\tilde{W}$  from (57).

Both detailed balance and duality symmetries are preserved under renormalisation if all terms in the action are retained. It is then crucial to follow Ref. [9] in choosing a basis for the RG equations that reflects this fact. The solution is to make the transformation defined by  $\tilde{V}$  in the previous section and to write as in (55)

$$\psi_{xt} = \frac{1}{2} \left( \phi_{xt} - \frac{\rho}{2} \right), \quad \psi_{xt}^\dagger = 2 \left( \phi_{xt}^\dagger - \frac{1}{2} \right). \quad (78)$$

Hence we can write the dynamical action in terms of these new fields:

$$S_{\text{FA}}[\psi, \psi^\dagger] = \int d^d x dt \psi_{xt}^\dagger \partial_t \psi_{xt} + \mu_0 (\psi_{xt}^\dagger - 1) (\psi_{xt} - \rho/4) (1 + l_0^2 \nabla^2 / 2) (\psi_{xt}^\dagger + 1) \psi_{xt} + \rho/4 \quad (79)$$

This is identical in form to  $S_{\text{AA}}$  as given in Equation (64), and so the FA model renormalises exactly as the AA model, consistent with their correlation functions

obeying the simple relation (60). The significance of the basis used is that the resulting RG equations respect both the detailed balance and duality symmetries of the FA model. If one makes any transform other than (78), using for example the standard shift  $\bar{\phi} = \phi^\dagger - 1$  as in Ref. [4], then these symmetries are obscured and one is led to the conclusion that the FA model is controlled by the DP fixed point between two and four dimensions.

#### 4.2. Simulations showing Gaussian scaling in $d = 3$

We now confirm our above exact predictions of mean-field (Gaussian) critical exponents in  $d > d_c = 2$  by equilibrium simulations of the FA model in  $d = 3$ . We explain how the duality relation (41) together with an appropriately adapted continuous time Monte Carlo (MC) algorithm allow us to probe critical properties well beyond the regime accessed in previous work. A comparison of our data with analytical scaling forms is also given.

A convenient observable for extracting the relaxation time scaling is the normalised two-point susceptibility  $\chi_2(t) = \langle \Delta E(t) \Delta E(0) \rangle / \langle \Delta E(0)^2 \rangle$  where  $\Delta E = E - \langle E \rangle$  denotes the fluctuation of the energy away from its equilibrium value. Since we only consider the stationary state dynamics of the FA model in this section, we drop the subscript ‘FA,eq’ on the averages. Substituting the simple form (1) of the energy function and using translational invariance,  $\chi_2(t)$  can be recast in the form

$$\chi_2(t) = \sum_i \frac{\langle n_i(t) n_j(0) \rangle - n_{\text{eq}}^2}{n_{\text{eq}}(1 - n_{\text{eq}})} = \sum_i \langle 0 | s_i^- e^{-\mathcal{L}_{\text{FA}} t} s_j^+ | 0 \rangle, \quad (80)$$

with  $j$  an arbitrary reference site and  $n_{\text{eq}} = \langle n_i \rangle$ , Equation (3). The second equality in (80) follows from the duality relation (41). It shows that the stationary state average defining  $\chi_2(t)$  has a dual counterpart in the dynamics near the empty state. This is a tremendously useful fact: instead of having to simulate an equilibrium system containing hundreds or even thousands of defects we simply initialise with a *single* defect at site  $j$ . According to (80),  $\chi_2(t)$  is then given by the probability that this state evolves under FA dynamics into one containing again a single defect (at an arbitrary site  $i$ ), that is any configuration with  $E = 1$ .

To measure with similar efficiency a dynamically growing lengthscale in the FA model one can consider the mean squared displacement associated with two-point correlations,

$$r_\chi^2(t) = \frac{1}{\chi_2(t)} \sum_i \|\mathbf{x}(i) - \mathbf{x}(j)\|^2 \frac{\langle n_i(t) n_j(0) \rangle - n_{\text{eq}}^2}{n_{\text{eq}}(1 - n_{\text{eq}})}. \quad (81)$$

Here  $\mathbf{x}(i)$  denotes the position vector of site  $i$ , and  $j$  is again an arbitrary reference site; we set the lattice constant to unity so that  $\mathbf{x}(i) \in \mathbb{Z}^d$ . Note that due to normalisation this lengthscale can exceed the equilibrium dynamical correlation length, which would conventionally be extracted from the maximum of  $\chi_2(t) r_\chi^2(t)$ . As in (80) we apply the duality (41) to map the stationary state average in (81) onto  $\langle 0 | s_i^- e^{-\mathcal{L}_{\text{FA}} t} s_j^+ | 0 \rangle$ ,

and perform simulations of the dual problem rather than the time-consuming direct equilibrium simulations.

The duality mapping increases the efficiency of an MC algorithm to such an extent that the limiting constraint in practical simulations is system size rather than computational speed. Although we initialise with just a single defect, its trajectory under FA dynamics explores the simulation box and must not be biased by finite size effects. For conventional, lattice based algorithms the required system size  $N = L^d$  can then quickly exhaust the available memory of standard computers (say 1Gb). To overcome this problem we used a coordinate-based variant of MC. Instead of storing the occupation numbers  $n_i$  of  $N$  lattice sites  $i$  we keep track of the actual coordinates  $\mathbf{x}_a$  of each defect  $a$  in the ‘virtual’ simulation box  $\{1, 2, \dots, L\}^d$ . The memory efficiency of this approach against a lattice based code is  $\mathcal{O}(M/N)$  if there are  $M$  defects. Hence it is useful for simulations of problems with low defect concentration, for instance, direct equilibrium simulations at low  $n_{\text{eq}}$  or the dual dynamics near the empty state. In analogy to lattice based codes [16, 17] one can set up a ‘reverse lookup scheme’ where continuous time MC steps have  $\mathcal{O}(1)$  computational complexity. This is accomplished by storing the list of defect coordinates  $\{\mathbf{x}_a\}_{a=1}^M$  in a hash table. So the problem of whether any site  $\mathbf{x}(i)$  in the virtual simulation box is occupied by a defect can be decided in  $\mathcal{O}(1)$  time, just as for a lattice based code. This coordinate-based continuous-time MC approach is memory efficient while yielding computational speeds comparable to a lattice based code. This allows us to exploit fully the simplifications afforded by (80) and (81).

Simulation results for branching rates  $c = 10^{-3}, 10^{-4}, 10^{-5}$  and  $10^{-6}$  are shown in Figures 3 and 4 below. We have used a formally infinite virtual simulation box so that via (80) and (81) we are probing the equilibrium dynamics of the FA model *in the thermodynamic limit*. In other words, our results are guaranteed to be free of finite size effects and can be compared directly to the scaling predictions (69) and (70). For this comparison we recall that at small defect densities the bosonic and hard core FA models have similar behaviour, so that  $\rho \propto \tilde{c} \approx c$  is proportional to  $c$ . Since we know that  $\beta = 1$  exactly, it is sufficient to show that  $z = 2$  and  $z\nu = 1$  to demonstrate Gaussian scaling. We first verify the dynamical critical exponent  $z = 2$  which implies for the growing length scale  $r_\chi(t)$ ,

$$r_\chi(t) \sim (D_0 t)^{1/z} \sim (ct)^{1/2}. \quad (82)$$

For all values of  $c$  considered the data in Figure 3 show a linear dependence of  $r_\chi^2(t)$  on  $ct$ , over up to eight decades in  $ct$ ; in fact our data are fully consistent with  $r_\chi^2(t) = 2dD_0t$  where  $d = 3$  and  $D_0 = c/2$ . This value of  $D_0$  confirms the expected scaling  $D_0 \sim c$ ; we return below to a derivation of the prefactor in  $D_0 = c/2$ . It should be emphasised that the kind of spatio-temporal scaling used here determines the dynamical exponent directly from its definition; measuring the ratio between exponents for the correlation length and relaxation time is a valid procedure only if the diffusion constant is slowly varying at criticality.

Consider next the simulation data for  $\chi_2(t)$  shown in the inset of Figure 4. Scaling

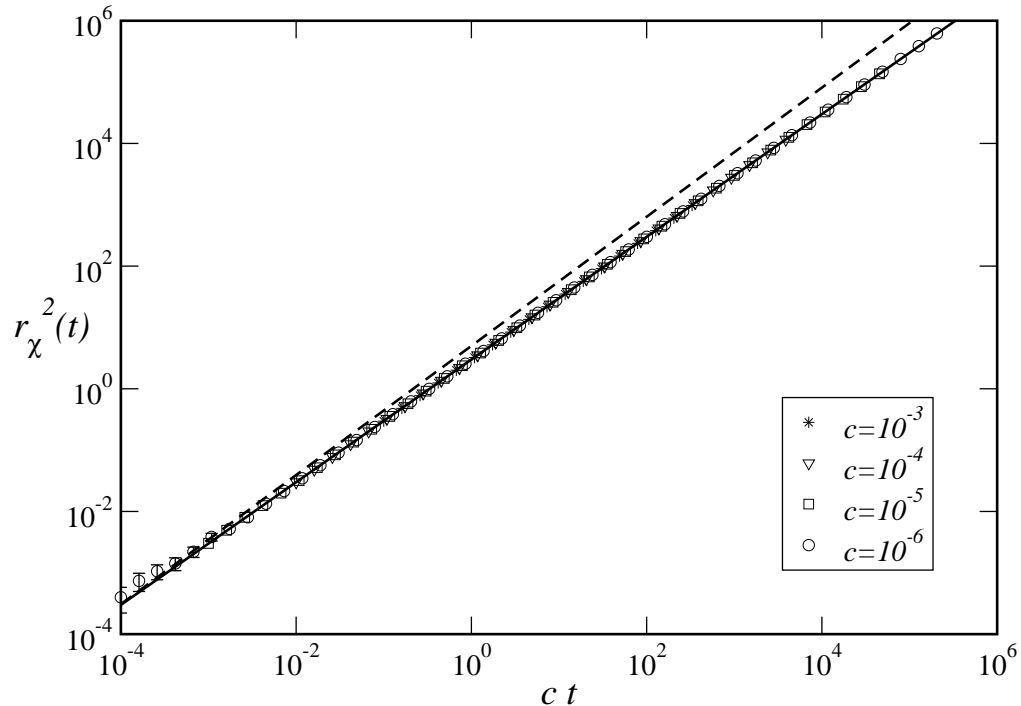


**Figure 3.** Simulation data (symbols) for equilibrium dynamics in the  $d = 3$  FA model with branching rates  $c = 10^{-3}, 10^{-4}, 10^{-5}$  and  $10^{-6}$  obtained from a coordinate-based continuous-time MC algorithm applied to the dual form of  $r_\chi^2(t)$ , Equation (81). Results are averaged over  $10^7, 10^6, 10^5$  and  $5 \times 10^4$  samples, respectively. The dynamical lengthscale increases according to a diffusive law  $r_\chi^2(t) = 2dD_0t$  and with diffusion constant  $D_0 = c/2$  (full line and symbols). Error bars are significantly smaller than the symbol-size except where they are shown explicitly (data for  $c = 10^{-6}$  with  $ct < 10^{-3}$ ). The dashed line represents DP scaling of the dynamical lengthscale as discussed in the main text; it is inconsistent with the data.

arguments predict that  $\chi_2(t)$  should be a universal function of  $t/\tau$ , with  $\tau$  the relaxation time. From (70) we expect for Gaussian exponents

$$\tau(c) \sim c^{-1-z\nu} = c^{-2}. \quad (83)$$

Collapse of data for  $\chi_2(t)$  under this prescription is shown in Figure 4. While there are still noticeable pre-asymptotic contributions at  $c = 10^{-3}$  the data for  $c = 10^{-4}$  and in particular  $c = 10^{-5}, 10^{-6}$  seem to have converged to the final scaling form of  $\chi_2(t)$  to within our numerical accuracy. To confirm the critical scaling in more detail we next give a theoretical analysis that predicts the precise shape of  $\chi_2(t)$  in the critical limit  $c \rightarrow 0$ .

#### 4.3. Scaling analysis for two-point functions in $d > 2$

We now show that the  $c \rightarrow 0$  limit of the equilibrium two-point susceptibility for FA models in  $d > 2$  dimensions is

$$\chi_2(t) = \exp(-\kappa_d c^2 t), \quad (84)$$

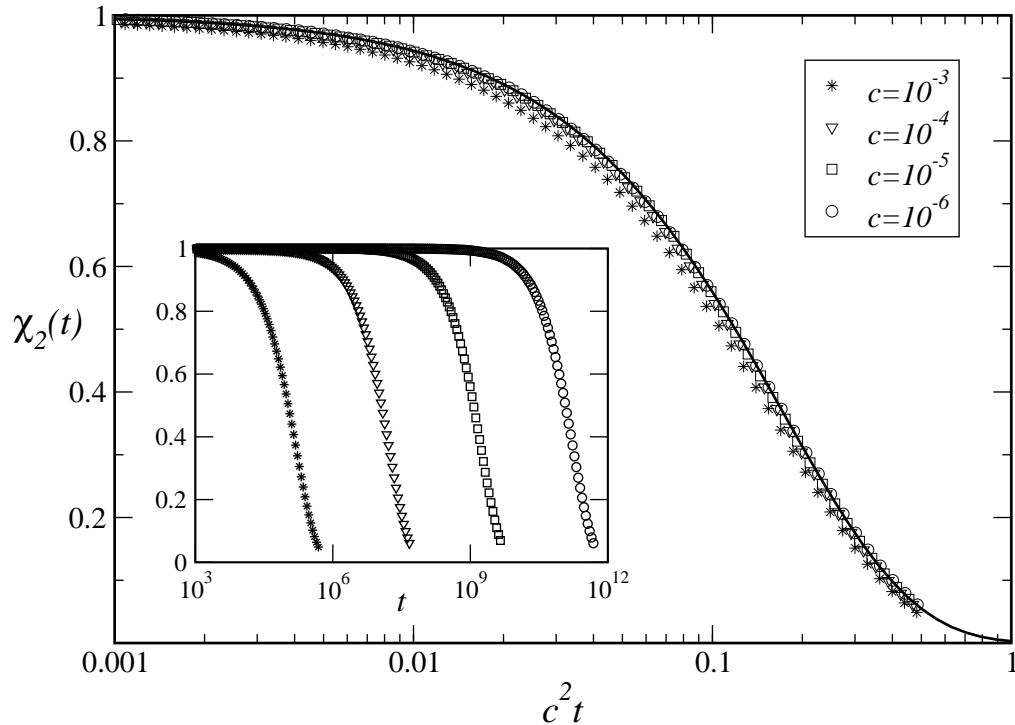


**Figure 4.** Simulation data obtained from the dual representation (80) of the two-point susceptibility  $\chi_2(t)$  and with the same parameters as in Figure 3. The inset shows  $\chi_2(t)$  versus  $t$ . At each  $c$  data are collected up to times  $t = 0.5/c^2$ , that is up to  $t = 0.5 \times 10^{12}$  for the lowest  $c$ . The main plot demonstrates data collapse with the Gaussian scaling of the relaxation time  $\tau \sim c^{-2}$ . The full line represents our analytical prediction for the  $c \rightarrow 0$  scaling of  $\chi_2(t)$ , Equation (84); there are no fit parameters. Error bars are largest for the data at  $c = 10^{-6}$ ; even there we estimate a relative error below 1%.

where  $\kappa_d = d[\mathcal{P}_d(2, 0, \dots, 0) + 2(d-1)\mathcal{P}_d(1, 1, 0, \dots, 0)]$ , and  $\mathcal{P}_d(\mathbf{x})$  is the probability that a pair of random walkers with initial separation  $\mathbf{x}$  will never meet: this function is considered in Appendix B. Equation (84) is consistent in particular with the scaling expectation that  $\chi_2(t)$  should be a function of  $t/\tau$  with  $\tau \sim c^{-2}$ . In  $d = 3$  and substituting the survival probabilities (B.6) and (B.7) one has  $\kappa_3 \approx 5.80961$ . The exact  $c \rightarrow 0$  scaling form (84) for this dimensionality is shown in Figure 4 and is in perfect agreement with our simulation data. The remainder of this subsection is devoted to the derivation of (84); we return to more general discussion in Section 4.4.

A systematic analysis of the dynamics in the critical limit  $c \rightarrow 0$  requires a careful distinction between the timescales involved. We will need unscaled time  $t$  as well as the scaled time variables  $x = ct$  and  $y = c^2t$  whose  $\mathcal{O}(1)$  increments correspond to time intervals  $\delta t$  of  $\mathcal{O}(c^{-1})$  and  $\mathcal{O}(c^{-2})$ , respectively. For time intervals  $\delta t = \mathcal{O}(1)$  the limit  $c \rightarrow 0$  is clear: the rate  $c$  for branching processes  $1_j 0_k \rightarrow 1_j 1_k$ , where  $k$  is a nearest neighbour (NN) of  $j$ , then vanishes. Only the coagulation processes  $1_j 1_k \rightarrow 1_j 0_k$  or  $1_j 1_k \rightarrow 0_j 1_k$  can then take place, each occurring with rate unity, and the lifetime of excited states like  $1_j 1_k$  that contain two (or more) NN defects is  $\mathcal{O}(1)$ .

The dynamics over intervals with  $\delta x = \mathcal{O}(1)$ , i.e.  $\delta t = \delta x/c = \mathcal{O}(c^{-1})$ , is rather different. Processes involving branching events are then possible. However, after such an initial event the rate for reverting to the original state is  $\mathcal{O}(1)$ , while the rate for an additional branching event is  $\mathcal{O}(c)$ . This implies that the probability for the latter to occur first is  $\mathcal{O}(c)$ . Since the rate for the first branching event is already  $\mathcal{O}(c)$ , the effective rate for a sequence of two branching events is then  $\mathcal{O}(c^2)$ . On our  $\mathcal{O}(c^{-1})$  timescales this type of process can be neglected, and we need only concern ourselves with processes involving a single branching event. One possible process is then  $1_j 0_k \rightarrow 1_j 1_k \rightarrow 0_j 1_k$ , with  $j, k$  NNs. Its rate is  $c \times \frac{1}{2}$ ,  $c$  being the branching rate and  $\frac{1}{2}$  the probability for the particular, subsequent coagulation (rather than  $1_j 1_k \rightarrow 1_j 0_k$ , which would take us back to the initial state). The probability for this process to occur during the interval  $\delta t$  is therefore  $\frac{1}{2}c\delta t = \frac{1}{2}\delta x$ . Note that as the lifetime of excited states is  $\mathcal{O}(1)$  as argued above, we have vanishing probability  $\mathcal{O}(c)$  of finding the system in an excited state  $1_j 1_k$  at any given moment in time. Therefore, in the limit  $c \rightarrow 0$ , the intermediate excited step of our process becomes invisible and we have *effective diffusion*  $1_j 0_k \rightarrow 0_j 1_k$  with probability  $\frac{1}{2}\delta x$ .

The second type of process allowed on the  $\mathcal{O}(c^{-1})$  timescale is the excitation of a defect at a site that has more than one NN defect, followed by a cascade of coagulation events leading to another configuration where all defects are isolated. Consider first the case where the new defect, at site  $k$  (say), has two NN defects at sites  $j$  and  $l$ , so that our process leads from  $1_j 1_k 1_l$  to  $1_j 0_k 0_l$  or  $0_j 1_k 0_l$  or  $0_j 0_k 1_l$ . The corresponding probabilities are  $\frac{1}{4}\delta x$ ,  $\frac{1}{2}\delta x$ ,  $\frac{1}{4}\delta x$ , respectively: after the initial excitation (probability  $2c\delta t = 2\delta x$ ) at site  $k$ , there is a probability of  $1/2$  that the defect at site  $k$ , which has twice the down-flip rate of those at  $j$  and  $l$ , will not flip down first. (If it does, we have returned to the original configuration and can ignore the process.) There is then probability  $1/2$  that  $j$  will flip before  $l$ , and probability  $1/2$  for each of the remaining defects to flip first, resulting in the overall probabilities given above.

To summarise the dynamics on the  $\mathcal{O}(c^{-1})$  timescale, we have diffusion  $1_j 0_k \rightarrow 0_j 1_k$  with rate  $\frac{1}{2}$  per interval of rescaled time  $x$ . The processes  $1_j 0_k 1_l \rightarrow 1_j 1_k 1_l \rightarrow \dots$  discussed above can then be represented consistently as produced by a diffusion event followed by (in the limit  $c \rightarrow 0$ ) instantaneous coagulation. For instance,  $1_j 0_k 1_l \rightarrow 1_j 0_k 0_l$  amounts to diffusion  $0_k 1_l \rightarrow 1_k 0_l$  (with rate  $\frac{1}{2}$ ) followed by coagulation  $1_j 1_k \rightarrow 1_j 0_k$  (which has probability  $\frac{1}{2}$  of occurring before  $1_j 1_k \rightarrow 0_j 1_k$ ), giving the overall rate  $\frac{1}{2} \times \frac{1}{2} = \frac{1}{4}$  obtained above. One can check that the same decomposition into diffusion and instantaneous coagulation also holds for processes involving an initial excitation at a site with more than two NN defects.

Our discussion so far leads to the following conclusions. Clearly any single-defect state  $s_j^+|0\rangle$  is blocked on the  $\mathcal{O}(1)$  timescale. Therefore  $\chi_2(t) = 1$  and  $r_\chi^2(t) = 0$  in equilibrium and for  $\mathcal{O}(1)$  times, according to the dual representations (80) and (81). But on the  $\mathcal{O}(c^{-1})$  timescale the defect diffuses away from its starting site  $j$ . This still predicts  $\chi_2(t) = 1$  since diffusion conserves the number of defects  $E = 1$ . The quantity  $r_\chi^2(t)$  in dual representation, on the other hand, now measures the mean squared



displacement of a single, diffusing defect which is given by  $r_x^2(t) = 2dD_0t$ . Our result that the diffusion rate is  $\frac{1}{2}$  in time units of  $x = ct$  tells us that  $D_0 = c/2$ . This is the exact low-density scaling of  $D_0$  and precisely what we found in our simulations; compare Figure 3.

Let us now turn to dynamics on the  $\mathcal{O}(c^{-2})$  timescale, corresponding to  $\delta y = c^2\delta t = \mathcal{O}(1)$ . During such a time interval there is now a nonzero probability for the occurrence of processes involving two successive branching events, where one defect is first excited next to an existing one and another defect is then created on a NN site to either of the other two. In order to determine the fate of this defect triple  $1_j1_k1_l$  we consider its evolution on the faster  $\mathcal{O}(c^{-1})$  timescale. This argument is analogous to the one above, where a defect pair is created on the  $\mathcal{O}(c^{-1})$  timescale but we have to look at  $\mathcal{O}(1)$  times to determine its relaxation. In further analogy we note that an arbitrarily small but nonzero increment  $\delta y$  on the  $\mathcal{O}(c^{-2})$  timescale corresponds to an infinite increment  $\delta x = \delta y/c$  of  $\mathcal{O}(c^{-1})$  time as  $c \rightarrow 0$ . The following possibilities then arise: because NN defects coagulate instantaneously on the  $\mathcal{O}(c^{-1})$  timescale there is a probability of  $\frac{1}{2}$  for immediate relaxation  $1_j1_k1_l \rightarrow 1_m$  where  $m = j$  or  $k$  or  $l$ . Subsequently the defect  $1_m$  diffuses with diffusion rate  $\frac{1}{2}$  for a time  $\delta x \rightarrow \infty$ , moving arbitrarily far from its initial position. With the remaining probability of  $\frac{1}{2}$  an instantaneous relaxation of the middle defect takes place,  $1_j1_k1_l \rightarrow 1_j0_k1_l$ . The defects  $1_j$  and  $1_l$  can now diffuse independently for an effectively infinite interval  $\delta x$  of  $\mathcal{O}(c^{-1})$ -time; if they do not coagulate in the process, their distance grows without bound and we can say the original defect has branched irreversibly. We derive in Appendix B the ‘survival probability’  $\mathcal{P}_d(\mathbf{x})$  for this outcome; here  $\mathbf{x} = \mathbf{x}(l) - \mathbf{x}(j)$  is the initial separation of the diffusing defects.

We can now assemble the probability  $\lambda\delta t$  that during a time interval  $\delta t = \delta y/c^2$  a single defect irreversibly branches into two defects. Starting from a single defect there is a rate  $c$  for branching on a given NN site. Since (on a hypercubic lattice in  $d$  dimensions) there are  $2d$  such states, the overall branching rate is  $2dc$ . The probability for a second branching event on a neighbouring site to take place before either of the two possible relaxations back to a single defect is  $c/2$ . A cluster of two NN defects has  $4d-2$  NN sites, two of which lead to a linear and  $4(d-1)$  to an angled defect triple  $1_j1_k1_l$ . Altogether the rate for creation of a linear triple is  $2dc^2$  while it is  $4d(d-1)c^2$  for an angled one. In either case, we need to multiply by the probability  $\frac{1}{2}$  of the middle defect  $k$  relaxing first, leading to a pair of next nearest neighbour (NNN) defects. In terms of the eventual survival probabilities  $\mathcal{P}_d(\mathbf{x})$  of this pair we thus obtain

$$\lambda = d[\mathcal{P}_d(2, 0, \dots, 0) + 2(d-1)\mathcal{P}_d(1, 1, 0, \dots, 0)]c^2. \quad (85)$$

This is a nontrivial result. To clarify its intuitive meaning, note that we are considering initially a single defect  $s_j^+|0\rangle$ . The following trajectories are then possible during a time interval  $\delta t = \delta x/c = \delta y/c^2$  on the  $\mathcal{O}(c^{-2})$  scale: (i) no branching occurs. The defect diffuses with rate  $\frac{1}{2}$  for a time  $\delta x = \delta y/c \rightarrow \infty$  in the  $c \rightarrow 0$  limit. The defect at the beginning and end of the interval  $\delta t$  are then completely decorrelated. (ii) With probability  $d(2d-1)c^2\delta t = d(2d-1)\delta y$  the defect branches into a pair of NNN defects.

Again, on the  $\mathcal{O}(c^{-1})$  timescale this pair has an infinite time  $\delta x$  available to diffuse through the system. (ii.a) There is a finite probability that the pair coagulates during this diffusive motion. In this case we have within the time interval  $\delta t$  a ‘bubble’ in the space-time diagram of the defect trajectories [3], where the initial defect separates into two but these re-coagulate shortly afterwards. The temporal extent of this bubble, i.e. the time during which the two defects exist, is  $\mathcal{O}(c^{-1})$ . The probability of detecting such a bubble on the  $\mathcal{O}(c^{-2})$  time scale is therefore vanishingly small in the limit  $c \rightarrow 0$ . This is in analogy to excited states becoming invisible on the  $\mathcal{O}(c^{-1})$  timescale. Hence the trajectories (i) and (ii.a) cannot be distinguished on the  $\mathcal{O}(c^{-2})$  timescale. (ii.b) The defects may diffuse forever ( $\delta x \rightarrow \infty$ ) without encountering each other; this means that the trajectory branches irreversibly on the  $\mathcal{O}(c^{-2})$  time scale. Due to the existence of bubbles the probability for this event,  $\lambda \delta t$ , is renormalised relative to the ‘bare’ probability  $d(2d - 1)c^2 \delta t$  for an initial branching event. Each defect in the resulting pair has travelled an infinite distance during  $\delta t$  and so completely decorrelates from the initial defect.

We can now make predictions for the dynamics on the  $\mathcal{O}(c^{-2})$  timescale. First we note that in  $d = 1, 2$  the survival probabilities  $\mathcal{P}_d(\mathbf{x})$  vanish, see Appendix B. Hence  $\lambda = 0$  and defect trajectories do not branch on the  $\mathcal{O}(c^{-2})$  timescale. However, in  $d > 2$  the  $\mathcal{P}_d(\mathbf{x})$  are finite, and hence so is  $\kappa_d = \lambda/c^2$ . Now  $\chi_2(t)$  is just the probability that the number of defects has not increased during the time interval  $t$ , which means that no irreversible branching processes have taken place. The rate for occurrence of the latter being  $\lambda$ , it follows that  $\chi_2(t) = \exp(-\lambda t) = \exp(-\kappa_d c^2 t)$ . This completes our derivation of Equation (84).

One can go further and extract the probability  $p_t(E)$  of having  $E \geq 1$  at time  $t$ . Since each irreversible branching event produces infinitely separated defects, these will then continue to branch *independently* in the same way. Thus, if  $E$  defects are present, the rate for generating an additional one by irreversible branching is  $E\lambda$ . This gives the master equation

$$\partial_t p_t(E) = (E - 1)\lambda p_t(E - 1) - E\lambda p_t(E). \quad (86)$$

This can be solved straightforwardly, for example by  $\mathcal{Z}$ -transform, to give

$$p_t(E) = e^{-\lambda t} (1 - e^{-\lambda t})^{E-1}. \quad (87)$$

The number of defects thus has an exponential distribution; the most likely outcome is  $E = 1$  at any time and has probability  $p_t(1) = \chi_2(t) = e^{-\lambda t}$ . The average number of defects, on the other hand, grows exponentially as  $\langle E \rangle_t = e^{+\lambda t}$ . We have checked in our simulations the full form of  $p_t(E)$  (data not shown), and found excellent agreement. The exponential increase in the number of defects limits the time range that can be conveniently simulated; the lowest value of  $\chi_2(t)$  that can be measured reliably is of the order of the inverse of the maximum number of defects one is prepared to track.

#### 4.4. Persistence functions and discussion of earlier data

In order to characterise a dynamical fixed point in the presence of a time-reversal symmetry, we must determine three independent exponents. One such set is  $(z, z\nu, \beta)$ . Our simulations as well as the scaling analysis have confirmed the RG prediction that  $z = 2$  and  $z\nu = 1$ ; further,  $\beta = 1$  is known rigorously from detailed balance. Consequently the scaling of the FA model in  $d = 3$  is Gaussian.

In Ref. [4], the authors found that the directed percolation (DP) fixed point is relevant to the FA model in three dimensions and at low temperatures. This conclusion seems unsatisfactory: we find no evidence for fluctuation corrections in our simulation data. Further, and more importantly, the DP fixed point is characterised by a diverging static lengthscale  $\xi$ : for a process in the DP universality class, one expects  $\langle n_i(0)n_j(0) \rangle_{\text{DP}} - \langle n \rangle_{\text{DP}}^2$  to be a scaling function of  $\|\mathbf{x}(i) - \mathbf{x}(j)\|/\xi$  where  $\xi$  diverges at criticality. On the other hand, detailed balance with respect to the non-interacting energy function (1) tells us that  $\langle n_i(0)n_j(0) \rangle_{\text{FA}} - \langle n \rangle_{\text{FA}}^2 \propto \delta_{ij}$  in the FA model. The absence of this diverging lengthscale in the FA model indicates that the underlying physics is different from that of the DP fixed point. Finally, we note that the exact result  $\beta = 1$  arises naturally from our RG treatment: this situation would appear more satisfactory than the argument of Ref. [4] that the exponents  $z$  and  $\nu$  should be given by their DP values while  $\beta$  is independently fixed to the non-DP value  $\beta = 1$  by detailed balance.

We argue that the conclusions of Ref. [4] regarding the DP fixed point are artefacts of an RG treatment that does not respect the presence of detailed balance and of the duality symmetry of the FA model; see also the comments after Equation (78). To remedy this, we have shown explicitly that writing the action as in (79) allows one to perform the RG analysis in a way that preserves these symmetries. We attribute the apparent fluctuation effects in the data for the relaxation time of Ref. [4], which were derived from the persistence function  $P(t)$ , to a combination of pre-asymptotic corrections in  $c$  and possible finite size effects. It should be emphasised that pre-asymptotic corrections are substantial: our simulations for  $\chi_2(t)$  show that branching rates of  $c = 10^{-3}$  are still too large to see the true critical scaling. Similar comments apply to the persistence function: we do find Gaussian scaling as shown in Figure 5, but to see this clearly requires very small  $c$ . Note that in order to obtain data for  $c = 10^{-5}$  and  $c = 10^{-6}$  we used virtual simulation boxes of size  $640^3$  and  $2000^3$ , respectively ‡. These cannot be reached by conventional lattice-based codes so that the data of Ref. [4] were of necessity taken from smaller systems, with potentially significant finite size effects. Although the DP exponents  $z_{\text{DP}} = 1.9$  and  $\nu_{\text{DP}} = 0.58$  in  $d = 3$  [8] differ

‡ While our coordinate-based MC algorithm is extremely memory efficient (in a  $2000^3$  lattice and at  $c = 10^{-6}$  there are on average only 8000 defects) keeping track of the persistence status is a problem for large lattices. We associate single bits with the persistence status of each lattice site so that we can track persistence in lattices up to  $1000^3$  using a memory block of 125Mb. At  $c = 10^{-6}$  we split the  $2000^3$  virtual simulation box into eight  $1000^3$  blocks but only track persistence in four of them to limit the memory requirement to 500Mb.

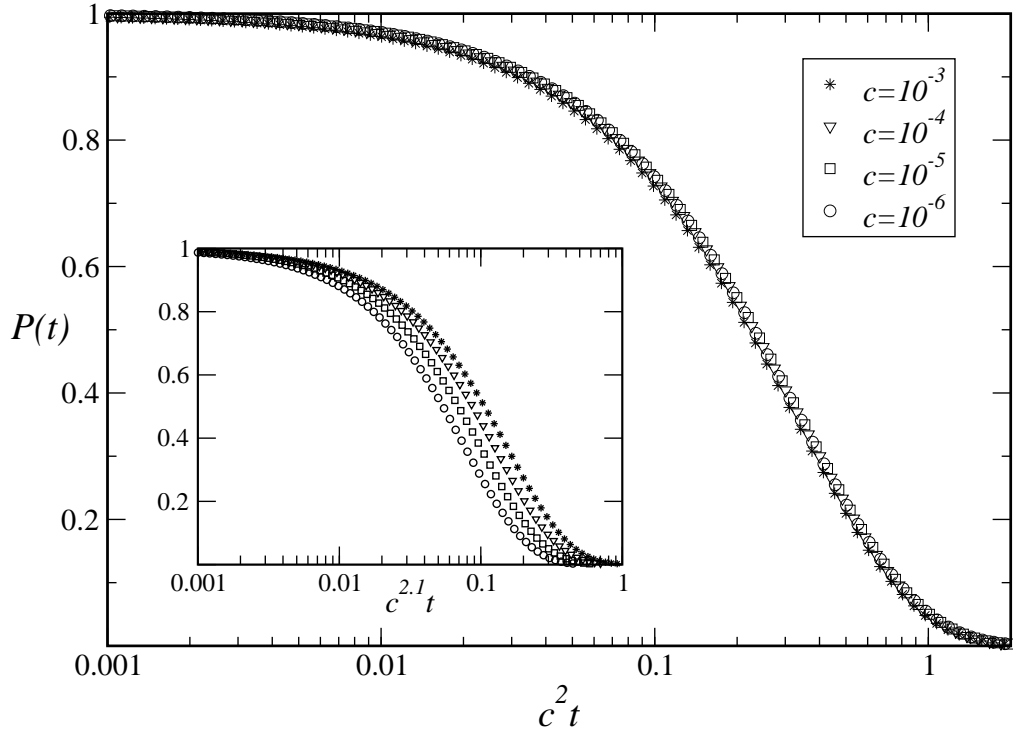


**Figure 5.** Simulation data (symbols) for the equilibrium persistence function  $P(t)$  in the  $d = 3$  FA model with branching rates  $c = 10^{-3}, 10^{-4}, 10^{-5}$  and  $10^{-6}$ . The main panel shows data collapse for Gaussian scaling of the relaxation time  $\tau \sim c^{-2}$ . The inset demonstrates that the data are inconsistent with DP scaling  $\tau_{\text{DP}} \sim c^{-2.105}$ . We used the coordinate-based continuous-time MC algorithm to measure  $P(t)$  in direct equilibrium simulations; since  $P(t)$  is effectively a correlation function of events at a continuous range of times, the duality relations for two-time correlations cannot be used. The size of the virtual simulation box is  $64^3, 200^3, 640^3$  and  $2000^3$ , respectively, which should be sufficient to avoid finite-size effects. Results are averaged over 1000, 100, 10 and 3 repeats, again in order of decreasing  $c$ . We expect relative errors of no more than 1% in the data shown.

only slightly from the Gaussian ones, our data clearly allow us to rule them out: the dashed line in Figure 3 represents DP scaling of the dynamical correlation length and is inconsistent with our data. The inset in Figure 5 demonstrates similarly that the persistence functions  $P(t)$  do not collapse when plotted against  $t/\tau_{\text{DP}}$  with the DP scaling  $\tau_{\text{DP}} \sim c^{-2.105}$ ; a rather similar picture – thus not shown – is obtained when plotting the two-point susceptibility  $\chi_2(t)$ , Figure 4, against  $t/\tau_{\text{DP}}$ .

We conclude that the DP fixed point is irrelevant for the FA model, for the same reason that it is irrelevant for the AA model and for parity conserving models of branching and annihilating random walks: these models possess extra symmetries that must be preserved in RG calculations and, in the case of the FA model, lead to Gaussian scaling. This conclusion parallels that of Cardy and Täuber [9], who showed that an early paper [18] on the parity conserving reaction-diffusion system ( $A \rightarrow 3A, 2A \rightarrow 0$ ) had produced a similar erroneous conclusion that the upper critical dimension was four and the exponents those of DP.

## 5. Conclusion

To summarise, we showed in Section 2 that the FA and AA models with hard core exclusion share the same correlation functions (at equilibrium, and considering a single time-difference). This was established by means of an exact mapping at the level of the master equation. An important generalisation which includes additional diffusive processes demonstrated that the same mapping connects more generally the reaction-diffusion models with reversible coagulation  $A + A \leftrightarrow A$  and reversible annihilation  $A + A \leftrightarrow 0$ . Further, we showed in Section 3 that the bosonic versions of the FA and AA models are appropriate effective theories for the low temperature limits of the hard core models and have analogous symmetries and relations between each other. Finally, in Section 4 we discussed the critical properties of the bosonic models using renormalisation group arguments. Implementing the mapping at the level of the field-theoretic action showed that the FA (and more generally  $A + A \leftrightarrow A$ ) model renormalises like the AA (or  $A + A \leftrightarrow 0$ ) model. We find that the directed percolation fixed point is irrelevant to the FA model, because of the presence of detailed balance and of an additional hidden symmetry inherited from the parity symmetry of the AA model. Instead, the  $A + A \leftrightarrow A$  model and its special case, the FA model, have upper critical dimension two; detailed balance together with the two exactly known scaling exponents is sufficient to find all exponents exactly also in  $d < 2$ .

From the point of view of reaction-diffusion systems and, more generally, non-equilibrium stochastic models, the most significant outcome of this work is the result that a hidden symmetry suppresses fluctuations in the  $A + A \leftrightarrow A$  model and lowers its upper critical dimension to  $d_c = 2$ . The mapping to  $A + A \leftrightarrow 0$  can, however, also be used to more quantitative purposes. For example, it enables one to calculate new exact results for two-time non-equilibrium correlation and response functions in  $d = 1$ ; we will report on these shortly [15]. The results of such an analysis are instructive also more generally with regard to non-equilibrium fluctuation-dissipation relations for activated dynamics [6]. In fact the FA model is an almost paradigmatic example of such dynamics, given that any evolution away from a metastable state containing only isolated defects requires the thermal excitation of additional defects.

From a different angle, one may ask what our results have to say about the usefulness of the FA model for capturing the qualitative behaviour of structural glasses [2, 3, 4]. We have seen that in the physically relevant case of three spatial dimensions, fluctuation effects at low defect densities are of a classical (mean-field, Gaussian) nature. Nevertheless, the models will still exhibit a degree of dynamical heterogeneity. Violations of the Stokes-Einstein relation [5] may also persist, but will be at most by a constant (rather than diverging) factor as  $c \rightarrow 0$ ; this is consistent with simulation results [19]. In summary, ‘glassy’ effects will be present, but probably rather weak. This is consistent with the fact that FA models also have relatively benign, Arrhenius-type increases of relaxation time scales at low temperature:  $\tau \sim c^{-2} \sim \exp(2/T)$  in  $d > 2$  as we saw above. These models are therefore suitable

at best for modelling for what are known as strong glasses. For fragile glasses with their super-Arrhenius timescale divergences, models with facilitation by more than one spin – or with directed constraints – will inevitably have to be used. Their much more cooperative dynamics [2] continues to make them physically attractive models for understanding non-trivial aspects of glassy dynamics.

## Acknowledgments

We thank L. Berthier, P. Calabrese, J. Cardy, J.-P. Garrahan, D. Reichman, R. Stinchcombe, U. Täuber and S. Whitlam for inspiring discussions. RLJ was supported by EPSRC grant no. GR/R83712/01.

## Appendix A. Large- $S$ expansion

To see mathematically the equivalence between the bosonic and hard core models in the limit of small particle densities, one can replace the spin-1/2 operators of the hard core case by their spin- $S$  analogues and perform a formal large- $S$  expansion, valid for states with small density. For example, we can define a new Master operator by generalising  $\mathcal{L}_{\text{FA}}$  from (18) to  $S > 1/2$ , as follows:

$$\mathcal{L}_{\text{SFA}} = \sum_{\langle ij \rangle} \left[ \frac{S + S_j^z}{2S} (S_i^+ - \sqrt{2S}) \frac{S - S_i^z}{2S} (S_i^- - \sqrt{2S}c) + (i \leftrightarrow j) \right], \quad (\text{A.1})$$

where  $S_i^z$  etc are operators in the spin- $S$  algebra. In the spin-half case we have  $S = 1/2$ ,  $(S + S_j^z)/(2S) = s_j^+ s_j^-$ ,  $(S - S_i^z)/(2S) = s_i^- s_i^+$  and so recover immediately  $\mathcal{L}_{\text{SFA}} = \mathcal{L}_{\text{FA}}$ .

The Master operator  $\mathcal{L}_{\text{SFA}}$  describes a system in which the number of particles on each site is restricted to the range  $0 \leq n_i \leq 2S$ ; the particle number operators are  $\hat{n}_i = S_i^z + S$ . Configurations  $\{n_i\}$  are mapped onto kets  $\prod_i (S_i^+ / \sqrt{2S})^{n_i} |0\rangle$  where  $|0\rangle$  is the empty state as before; since  $\hat{n}_i |0\rangle = 0$  is equivalent to  $S_i^z |0\rangle = -S |0\rangle$  this state is, in spin language, fully polarised in the ( $-z$ ) direction. Probabilities for transitions between states in some time interval  $t$  are then given by

$$P_{\{n'_i\} \leftarrow \{n_i\}}(t) = \langle 0 | \left[ \prod_i \frac{1}{\Gamma_{S, n'_i}} \left( \frac{S_i^-}{\sqrt{2S}} \right)^{n'_i} \right] e^{-\mathcal{L}_{\text{SFA}} t} \left[ \prod_i \left( \frac{S_i^+}{\sqrt{2S}} \right)^{n_i} \right] |0\rangle \quad (\text{A.2})$$

where we have introduced the coefficients  $\Gamma_{S, n} = (2S)^{-n} \langle 0 | (S_i^-)^n (S_i^+)^n |0\rangle$  for ease of writing. These obey the recursion  $\Gamma_{S, n+1} = \Gamma_{S, n} (n+1) [1 - n/(2S)]$ , yielding explicitly  $\Gamma_{S, n} = n! (2S)! / [(2S - n)! (2S)^n]$ . From (A.2), conservation of probability requires that

$$\langle 0 | \left[ \prod_i \sum_{n_i=0}^{2S} \frac{1}{\Gamma_{S, n'_i}} \left( \frac{S_i^-}{\sqrt{2S}} \right)^{n'_i} \right] \mathcal{L}_{\text{SFA}} = 0 \quad (\text{A.3})$$

which can be verified by direct calculation. We identify this left eigenstate as the projection state; it is analogous to  $\langle e |$  and  $\langle \tilde{e} |$  for hard core and bosonic models, respectively.

Using  $S_i^+(S_i^+/\sqrt{2S})^n|0\rangle = \sqrt{2S}(S_i^+/\sqrt{2S})^{n+1}|0\rangle$  and  $S_i^-(S_i^+/\sqrt{2S})^n|0\rangle = \sqrt{2S} \times n[1 - n/(2S)](S_i^+/\sqrt{2S})^{n-1}|0\rangle$  one easily checks that the microscopic rates in the model defined by  $\mathcal{L}_{\text{SFA}}$  are

$$\begin{aligned} n_i n_j &\rightarrow (n_i + 1)n_j, & \text{rate } cn_j[1 - n_i/(2S)], \\ (n_i + 1)n_j &\rightarrow n_i n_j, & \text{rate } n_j(n_i + 1)[1 - n_i/(2S)]^2 \end{aligned} \quad (\text{A.4})$$

These obey detailed balance with respect to the stationary state

$$P(\{n_i\}) \propto \prod_i \frac{c^{n_i}}{\Gamma_{S,n_i}}. \quad (\text{A.5})$$

We have defined a family of interpolating models with increasing  $S$  that allow us to gradually remove the hard core constraints. We will now use a large- $S$  expansion to show that the models without constraints coincide with the bosonic models defined above. As long as there is no qualitative change in behaviour on increasing  $S$  we therefore expect the bosonic models to be suitable effective theories for the low temperature (small  $c$ ) behaviour of the hard core ones. An example of a qualitative change that would render the large- $S$  expansion invalid is a transition to a quantum disordered state as  $S$  is reduced [20]: there is clearly no such singular behaviour here. Indeed, in our case the stationary states (A.5) of the models are known for general  $S$ . Bearing in mind that  $\Gamma_{S,0} = \Gamma_{S,1} = 1$ , they are all of effectively the same form if  $c$  is small so that only states with  $n_i = 0, 1$  have significant probability.

Our claim that the above interpolating model becomes equivalent to the bosonic one in the limit  $S \rightarrow \infty$  can be confirmed directly from (A.4): as long as  $c$  is small so that the relevant values of  $n_i$  stay small compared to  $2S$ , the large- $S$  limit of the transition rates gives the bosonic model (4). Correspondingly, the stationary state (A.5) becomes the bosonic one in this limit since  $\Gamma_{S,n} \rightarrow n!$ .

More formally, one can establish the large- $S$  limit of our interpolating model by looking at the Hermitian version of the Liouvillian. Using detailed balance this is defined as  $H_{\text{SFA}} = [\prod_i c^{-\hat{n}_i/2}] \mathcal{L}_{\text{SFA}} [\prod_i c^{\hat{n}_i/2}]$  or explicitly

$$H_{\text{SFA}} = \sum_{\langle ij \rangle} \left[ \frac{S + S_j^z}{2S} (S_i^+ - \sqrt{2Sc}) \frac{S - S_i^z}{2S} (S_i^- - \sqrt{2Sc}) + (i \leftrightarrow j) \right] \quad (\text{A.6})$$

Then we can use the Holstein-Primakov representation [21]

$$S_i^z = a_i^\dagger a_i - S, \quad S_i^+ = a_i^\dagger (2S - a_i^\dagger a_i)^{1/2} \quad (\text{A.7})$$

and take the large- $S$  limit by approximating  $2S - a_i^\dagger a_i = 2S - \hat{n}_i \approx 2S$  everywhere. This assumes again that  $c$  is small enough so that all relevant states have particle numbers  $n_i \ll 2S$  at each site. In spin language, all the states of interest are then localised on a small part of the surface of the spin sphere, and the non-trivial structure of the spin algebra can be neglected in favour of a simple bosonic one via  $S_i^+ \approx \sqrt{2S} a_i^\dagger$ . Taking the  $S \rightarrow \infty$  limit as explained, we get

$$H_{\text{SFA}} \simeq \sum_{\langle ij \rangle} [a_j^\dagger a_j (a_i^\dagger - \sqrt{c})(a_i - \sqrt{c}) + (i \leftrightarrow j)]. \quad (\text{A.8})$$

This coincides with the Hermitian form (49) of the Liouvillian of the bosonic FA model as claimed, with the expected correspondence  $\tilde{c} = c$ . An exactly analogous procedure can be applied to construct a family of models that interpolates smoothly between the hard core and bosonic AA models. We therefore expect that the bosonic FA and AA models will be appropriate effective theories for their hard core counterparts at small particle densities.

## Appendix B. Random walk survival probabilities

For the scaling analysis of equilibrium correlation functions given in Section 4.3 we required particular random walk survival probabilities; these are derived in the following. Consider a pair of diffusing defects. We can think of these as random walkers on a  $d$ -dimensional hypercubic lattice  $\mathbb{Z}^d$ ; whenever they occupy NN sites, where their positions have distance  $\|\mathbf{x}_2 - \mathbf{x}_1\| = 1$ , they coagulate instantaneously. We are interested in the probability  $\mathcal{P}_d(\mathbf{x})$  that the walkers survive to infinite time, i.e. never coagulate. This survival probability depends on the spatial dimensionality  $d$  and on the initial separation  $\mathbf{x} = \mathbf{x}_2 - \mathbf{x}_1$  of the walkers. The distance vector  $\mathbf{x}_2 - \mathbf{x}_1$  also performs a random walk, with twice the effective diffusion constant. The problem is therefore to calculate the probability  $\mathcal{P}_d(\mathbf{x})$  that a random walker starting from position  $\mathbf{x}$  will never reach one of the NN sites of the origin. If we picture these sites as absorbing, then  $\mathcal{Q}_d(\mathbf{x}) = 1 - \mathcal{P}_d(\mathbf{x})$  is the probability that the walker is absorbed eventually; for absorption at the origin itself, these quantities are well known.

The key insight is that, in its first step, the walker randomly moves to one of the NN sites of  $\mathbf{x}$ ; we write these as  $\mathbf{y} \in N(\mathbf{x})$ . The absorption probability starting from  $\mathbf{x}$  is therefore the average of those that would be obtained when starting from any of these NN sites:

$$\mathcal{Q}_d(\mathbf{x}) = \frac{1}{2d} \sum_{\mathbf{y} \in N(\mathbf{x})} \mathcal{Q}_d(\mathbf{y}). \quad (\text{B.1})$$

The only exception to this relation is the case where  $\mathbf{x}$  itself is already an absorption site so that  $\mathcal{Q}_d(\mathbf{x}) = 1$ . We can correct for this by adding a source term at these sites; the latter then has to be set at the end of the calculation to give the correct values of  $\mathcal{Q}_d(\mathbf{x})$  at the absorption sites. Since all lattice directions are equivalent, all  $2d$  source terms will be equal and we can write

$$\mathcal{Q}_d(\mathbf{x}) = \frac{1}{2d} \left[ v \delta_{\mathbf{x}, N(\mathbf{0})} + \sum_{\mathbf{y} \in N(\mathbf{x})} \mathcal{Q}_d(\mathbf{y}) \right]. \quad (\text{B.2})$$

For the Fourier components  $Q_{\mathbf{k}} = \sum_{\mathbf{x}} \mathcal{Q}_d(\mathbf{x}) e^{-i\mathbf{k} \cdot \mathbf{x}}$  this gives

$$Q_{\mathbf{k}} = v \frac{\sum_{\alpha} \cos k_{\alpha}}{d - \sum_{\alpha} \cos k_{\alpha}} = v \left[ -1 + d \int_0^{\infty} d\tau e^{-\tau(d - \sum_{\alpha} \cos k_{\alpha})} \right], \quad (\text{B.3})$$



where  $\alpha = 1, \dots, d$  labels the lattice directions. The second, integral form of the result makes the reverse Fourier transform simple:

$$\mathcal{Q}_d(\mathbf{x}) = v \left[ -\delta_{\mathbf{x}, \mathbf{0}} + d \int_0^\infty d\tau e^{-d\tau} \prod_\alpha I_{x_\alpha}(\tau) \right], \quad (\text{B.4})$$

where the  $I_n$  are modified Bessel functions,  $I_n(\tau) = \frac{1}{2\pi} \int_0^{2\pi} dk \cos(nk) e^{\tau \cos k}$ . Choosing  $v$  to ensure that  $\mathcal{Q}_d(\mathbf{x}) = 1$  for  $\mathbf{x} \in N(\mathbf{0})$  then gives for  $\mathbf{x} \neq \mathbf{0}$ ,

$$\mathcal{Q}_d(\mathbf{x}) = 1 - \mathcal{P}_d(\mathbf{x}) = \frac{\int_0^\infty d\tau e^{-d\tau} \prod_\alpha I_{x_\alpha}(\tau)}{\int_0^\infty d\tau e^{-d\tau} I_0^{d-1}(\tau) I_1(\tau)}. \quad (\text{B.5})$$

We remark that for  $\mathbf{x} = \mathbf{0}$  one finds, by retaining the  $\delta_{\mathbf{x}, \mathbf{0}}$  term, that  $\mathcal{Q}_d(\mathbf{0}) = 1$  as it must be: starting from the origin, already the first move reaches an absorption site. Given the derivation of (B.5), it is not too surprising that the result is similar to that for the standard case of absorption at the origin, where one finds the same expression but with the denominator replaced by  $\int d\tau e^{-d\tau} I_0^d(\tau)$ .

In dimensions  $d = 1, 2$  the original pair of walkers always coagulate eventually, regardless of the initial separation and thus  $\mathcal{P}_d(\mathbf{x}) = 0$ . (This can be seen formally from the fact that both the numerator and denominator integrals in (B.5) are dominated by their divergent tails; these have  $\mathbf{x}$ -independent prefactors, giving  $\mathcal{Q}_d(\mathbf{x}) = 1$ .) In  $d > 2$ , on the other hand, Equation (B.5) yields a nonzero probability  $\mathcal{P}_d(\mathbf{x})$  that the walkers survive indefinitely. The two particular values we need in the main text are

$$\mathcal{P}_3(2, 0, 0) = 1 - \frac{\int_0^\infty d\tau e^{-3\tau} I_0^2(\tau) I_2(\tau)}{\int_0^\infty d\tau e^{-3\tau} I_0^2(\tau) I_1(\tau)} \approx 0.50166, \quad (\text{B.6})$$

$$\mathcal{P}_3(1, 1, 0) = 1 - \frac{\int_0^\infty d\tau e^{-3\tau} I_0(\tau) I_1^2(\tau)}{\int_0^\infty d\tau e^{-3\tau} I_0^2(\tau) I_1(\tau)} \approx 0.35872. \quad (\text{B.7})$$

The rather significant difference between the numerical values (B.6) and (B.7) has a simple reason: when starting at initial separation  $\mathbf{x} = (1, 1, 0)$  there are 12 possible first moves since each walker has 6 NN sites to move to. Out of these, 4 lead to the walkers being on NN sites where they coagulate instantaneously, while for  $\mathbf{x} = (2, 0, 0)$  only 2 moves produce this outcome. There are similar differences in subsequent moves which accumulate to the numbers given above.

## References

- [1] G. H. Fredrickson and H. C. Andersen, Phys. Rev. Lett **53**, 1244 (1984).
- [2] F. Ritort and P. Sollich, Adv. Phys **52**, 219 (2003).
- [3] J. P. Garrahan and D. Chandler, Phys. Rev. Lett. **89**, 035704 (2002); Proc. Natl. Acad. Sci. U.S.A. **100**, 9710 (2003).
- [4] S. Whitelam, L. Berthier and J. P. Garrahan, Phys. Rev. Lett. **92**, 185705 (2004); Phys. Rev. E **71**, 026128 (2005).
- [5] Y. Jung, J.P. Garrahan and D. Chandler, Phys. Rev. E **69**, 061205 (2004).
- [6] P. Mayer, S. Leonard, L. Berthier, J.P. Garrahan and P. Sollich, Phys. Rev. Lett., in press, and preprint cond-mat/0508686.
- [7] C. Toninelli, M. Wyart, L. Berthier, G. Biroli, J.P. Bouchaud, Phys. Rev. E **71**, 041505 (2005).

- [8] H. Hinrichsen, *Adv. Phys.* **49**, 815 (2000).
- [9] J. L. Cardy and U. C. Täuber, *J. Stat. Phys.* **90**, 1 (1998)
- [10] R. Stinchcombe, *Adv. Phys.* **50**, 431 (2001).
- [11] K. Krebs, M. P. Pfannmüller, B. Wehefritz and H. Hinrichsen, *J. Stat. Phys.* **78**, 1429 (1995).
- [12] M. Henkel, E. Orlandini and J. Santos, *Ann. Phys.* **259**, 163 (1997).
- [13] I. S. Graham, L. Piché and M. Grant, *J. Phys. Cond. Matt.* **5**, 6491 (1993); *Phys. Rev. E* **55**, 2132 (1997).
- [14] M. Doi, *J. Phys. A* **9**, 1479 (1976); L. Peliti, *J. Phys. (Paris)* **46**, 1469 (1984).
- [15] P. Mayer and P. Sollich, in preparation.
- [16] A. B. Bortz, M. H. Kalos and J. L. Lebowitz, *J. Comput. Phys.* **17**, 10 (1975).
- [17] M. E. J. Newman and G. T. Barkema, *Monte Carlo Methods in Statistical Physics* (Oxford University Press, New York, Oxford, 1999).
- [18] P. Grassberger, *J. Phys. A* **22**, L1103 (1989).
- [19] J.P. Garrahan, private communication.
- [20] S. Sachdev, *Quantum Phase Transitions* (Cambridge University Press, Cambridge, UK, 1999).
- [21] T. Holstein and H. Primakoff, *Phys. Rev.* **58**, 1098 (1940)